

---

# PLANE: Representation Learning over Planar Graphs

---

Radoslav Dimitrov\* Zeyang Zhao<sup>1</sup>\* Ralph Abboud İsmail İlkan Ceylan<sup>1</sup>

<sup>1</sup>Department of Computer Science, University of Oxford  
 contact@radoslav11.com zeyzang.zhao@cs.ox.ac.uk  
 ralph@alphabb.ai ismail.ceylan@cs.ox.ac.uk

## Abstract

Graph neural networks are prominent models for representation learning over graphs, where the idea is to iteratively compute representations of nodes of an input graph through a series of transformations in such a way that the learned graph function is isomorphism invariant on graphs, which makes the learned representations *graph invariants*. On the other hand, it is well-known that graph invariants learned by these class of models are *incomplete*: there are pairs of non-isomorphic graphs which cannot be distinguished by standard graph neural networks. This is unsurprising given the computational difficulty of graph isomorphism testing on general graphs, but the situation begs to differ for special graph classes, for which efficient graph isomorphism testing algorithms are known, such as planar graphs. The goal of this work is to design architectures for *efficiently* learning *complete* invariants of planar graphs. Inspired by the classical planar graph isomorphism algorithm of Hopcroft and Tarjan, we propose PLANE as a framework for planar representation learning. PLANE includes architectures which can learn *complete* invariants over planar graphs while remaining practically scalable. We empirically validate the strong performance of the resulting model architectures on well-known planar graph benchmarks, achieving multiple state-of-the-art results.

## 1 Introduction

Graphs are standard for representing relational data in a wide range of domains, including physical [53], chemical [18, 36], and biological [22, 67] systems, which led to increasing interest in machine learning over graphs. Graph neural networks (GNNs) [24, 51] have become prominent for graph machine learning for a wide range of tasks, owing to their capacity to explicitly encode desirable relational inductive biases [6]. GNNs iteratively compute representations of nodes of an input graph through a series of transformations in such a way that the learned graph-level function represents a *graph invariant*: a property of graphs which is preserved under all isomorphic transformations.

Learning functions on graphs is challenging for various reasons, particularly since the learning problem contains the infamous graph isomorphism problem, for which the best known algorithm, given in a breakthrough result by Babai [4], runs in quasi-polynomial time. A large class of GNNs can therefore only learn *incomplete* graph invariants for scalability purposes. In fact, standard GNNs are known to be at most as expressive as the 1-dimensional Weisfeiler-Leman algorithm (1-WL)[58] in terms of distinguishing power [45, 62]. There are simple non-isomorphic pairs of graphs, such as the pair shown in Figure 1, which cannot be distinguished by 1-WL and by a large class of GNNs. This limitation motivated a large body of work aiming to explain and overcome the expressiveness barrier of these architectures [1, 5, 7, 9, 11, 16, 37, 42, 43, 45, 50].

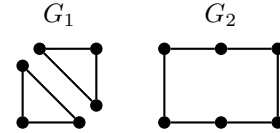


Figure 1: The graphs  $G_1$  and  $G_2$  are indistinguishable by 1-WL.

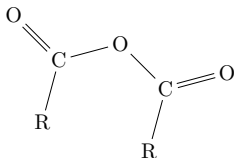


Figure 2: Acid anhydride as a planar graph with node and edge types.

The expressiveness limitations of standard GNNs already apply on planar graphs, since, e.g., the graphs  $G_1$  and  $G_2$  from Figure 1 are planar. There are, however, efficient and complete graph isomorphism testing algorithms for planar graphs [29, 30, 41], which motivates an aligned design of dedicated architectures with better properties over planar graphs. Building on this idea, this paper proposes architectures for *efficiently learning complete invariants* over planar graphs.

Planar graphs are very prominent structures, and appear, e.g., in road networks [61], circuit design [8], and most importantly, in biochemistry [54]. Molecules are commonly encoded as planar graphs with node and edge types, as shown in Figure 2, which enables the application of many graph machine learning architectures on biochemistry tasks. For example, *all* molecule datasets in OGBG [33] fully consist of planar graphs. Biochemistry has been a very important application domain for both classical graph isomorphism testing<sup>1</sup> and for graph machine learning. Therefore, by designing architectures learning *complete invariants* over planar graphs, our work unlocks the full potential of both these domains.

The contributions of this work can be summarized as follows:

- Building on the classical literature of planar graph isomorphism testing, we introduce PLANE as a framework for learning *isomorphism-complete* invariant functions over planar graphs.
- We derive a model architecture, BASEPLANE, and prove that it is a *complete* learning algorithm on planar graphs: BASEPLANE can distinguish any pair of non-isomorphic planar graphs.
- We use an existing synthetic dataset, EXP [1], and experimentally verify the expressive power of BASEPLANE. Moreover, we design a graph regression task, where the goal is to predict the (normalized) graph clustering on a subset of the molecular dataset QM9 [48]. In strong contrast to classical architectures, BASEPLANE can predict the clustering coefficients almost perfectly.
- We experiment on real-world datasets and obtain multiple state-of-the-art results on molecular datasets, suggesting the strength of BASEPLANE.

The full technical details of the algorithms, and proofs are delegated to the appendix of this paper.

## 2 A primer on graphs, invariants, and graph neural networks

**Graphs and connectivity.** Consider simple, undirected graphs  $G = (V, E, \zeta)$ , where  $V$  is a set of nodes,  $E \subseteq V \times V$  is a set of edges, and  $\zeta : V \rightarrow \mathbb{C}$  is a (coloring) function. If the range of this map is  $\mathbb{C} = \mathbb{R}^d$ , we refer to it as a *d-dimensional feature map*. A graph is *connected* if there is a path between any two nodes and disconnected otherwise. A graph is *biconnected* if it cannot become disconnected by removing any single node. A graph is *triconnected* if the graph cannot become disconnected by removing any two nodes. A graph is *planar* if it can be drawn on a plane such that no two edges intersect.

**Components.** A *biconnected component* of a graph  $G$  is a maximal biconnected subgraph. Any connected graph  $G$  decomposes into a tree of biconnected components called the *Block-Cut tree* of the graph, which we denote as  $\text{BLOCKCUT}(G)$ . The blocks are attached to each other at shared nodes called *cut nodes* or *articulation points*. A *triconnected component* of a graph  $G$  is a maximal triconnected subgraph. Triconnected components of a graph  $G$  can also be represented in terms of a tree, known as the *SPQR tree*, which we denote as  $\text{SPQR}(G)$ . It is useful to refer to components of a graph in terms of a set. Given a graph  $G$ , we denote by  $\sigma^G$  the set of all components induced from the nodes of  $\text{SPQR}(G)$ , and by  $\pi^G$  the set of all biconnected components of  $G$ . Moreover, we denote by  $\sigma_u^G$  the set of all SPQR components of  $G$  where  $u$  appears as a node, and by  $\pi_u^G$  the set of all biconnected components of  $G$  where  $u$  appears as a node.

**Labeled trees.** We sometimes refer to rooted, undirected, labeled trees  $\Gamma = (V, E, \zeta)$ , where the canonical root node is given as one of tree’s *centroids*: a node with the property that none of its branches contains more than half of the other nodes. We denote by  $\text{ROOT}(\Gamma)$  the canonical root of  $\Gamma$ ,

<sup>1</sup>Graph isomorphism first appears in the chemical documentation literature [49], as the problem of matching a molecular graph against a database of such graphs; see, e.g., Grohe and Schweitzer [27] for a recent survey.

and define the *depth*  $d_u$  of a node  $u$  in the tree as the node’s minimal distance from the canonical root. The *children* of a node  $u$  is the set  $\chi(u) = \{v \mid (u, v) \in E, d_v = d_u + 1\}$ . The *descendants* of a node  $u$  is given by set of all nodes reachable from  $u$  through a path of length  $k \geq 0$  such that the node at position  $j + 1$  has one more depth than the node at position  $j$ , for every  $0 \leq j \leq k$ . Given a rooted tree  $\Gamma$  and a node  $u$ , the *subtree* of  $\Gamma$  rooted at node  $u$  is the tree induced by the descendants of  $u$ , which we denote by  $\Gamma_u$ . For technical convenience, we allow the induced subtree  $\Gamma_u$  of a node  $u$  even if  $u$  does not appear in the tree  $\Gamma$ , in which case  $\Gamma_u$  is the empty tree.

**Node and graph invariants.** An *isomorphism* from a graph  $G = (V, E, \zeta)$  to a graph  $G' = (V', E', \zeta')$  is a bijection  $f : V \rightarrow V'$  such that  $\zeta(u) = \zeta'(f(u))$  for all  $u \in V$ , and  $(u, v) \in E$  if and only if  $(f(u), f(v)) \in E'$ , for all  $u, v \in V$ . A *node invariant* is a function  $\xi$  that associates with each graph  $G = (V, E, \zeta)$  a function  $\xi(G)$  defined on  $V$  such that for all graphs  $G$  and  $G'$ , all isomorphisms  $f$  from  $G$  to  $G'$ , and all nodes  $u \in V$ , it holds that  $\xi(G)(u) = \xi(G')(f(u))$ . A *graph invariant* is a function  $\xi$  defined on graphs such that  $\xi(G) = \xi(G')$  for all isomorphic graphs  $G$  and  $G'$ . We can derive a graph invariant  $\xi$  from a node invariant  $\xi'$  by mapping each graph  $G$  to the multiset  $\{\{\xi'(G)(u) \mid u \in V\}\}$ . We say that a graph invariant  $\xi$  *distinguishes* two graphs  $G$  and  $G'$  if  $\xi(G) \neq \xi(G')$ . If a graph invariant  $\xi$  distinguishes  $G$  and  $G'$  then there is no isomorphism from  $G$  to  $G'$ . If the converse also holds, then  $\xi$  is a *complete* graph invariant. We can speak of (in)completeness of invariants on special classes of graphs, e.g., the 1-WL computes an incomplete invariant on general graphs, but it is well-known to compute a complete invariant on trees [25].

**Message passing neural networks.** A vast majority of graph neural networks are instances of *message passing neural networks (MPNNs)* [23]. Given an input graph  $G = (V, E, \zeta)$ , an MPNN sets, for each node  $u \in V$ , an initial node representation  $\zeta(u) = \mathbf{h}_u^{(0)}$ , and iteratively computes representations  $\mathbf{h}_u^{(\ell)}$  for a fixed number of layers  $0 \leq \ell \leq L$  as:

$$\mathbf{h}_u^{(\ell+1)} := \phi \left( \mathbf{h}_u^{(\ell)}, \psi(\mathbf{h}_u^{(\ell)}, \{\{\mathbf{h}_v^{(\ell)} \mid v \in N_u\}\}) \right),$$

where  $\phi$  and  $\psi$  denote the *update* and *aggregation* functions, respectively, and  $N_u$  denotes the neighborhood of node  $u$ .

Node representations can be *pooled* to obtain graph-level embeddings by, e.g., summing all node embeddings. We denote by  $\mathbf{z}^{(L)}$  the resulting graph-level embeddings. In this case, an MPNN can be viewed as an encoder that maps each graph  $G$  to a representation  $\mathbf{z}^{(L)}$ , computing a graph invariant.

### 3 Related work

The expressive power of MPNNs is upper bounded by 1-WL [45, 62] in terms of distinguishing graphs, and by the logic  $\mathcal{C}^2$  in terms of capturing functions over graphs [5]. Therefore, substantial research has been conducted to improve on these bounds. One notable direction has been to enrich node features, most prominently with unique node identifiers [42, 64], random discrete colors [16], and even random noisy dimensions [1, 50]. Another line of work proposes *higher-order* architectures [37, 43–45] based on higher-order tensors [44], or a higher-order form of message passing [45], which typically align with a  $k$ -dimensional variant of the WL test, for some  $k > 1$ . Higher-order architectures, however, are generally not scalable, and most existing models are therefore upper bounded by 2-WL (or, *oblivious* 3-WL); see Grohe [26] for details of the  $k$ -WL hierarchy and its correspondence with higher-order GNNs. Another body of work is based on sub-graph sampling [7, 9, 11, 55], with pre-set sub-graphs used within model computations. These approaches can yield substantial expressiveness improvements, e.g., CWN [9] is more powerful than 2-WL (or oblivious 3-WL), but these improvements typically rely on manual sub-graph selection, and require running expensive pre-computations. Finally, MPNNs have been extended to incorporate other graph kernels, namely shortest paths [2, 63], random walks [46, 47] and nested color refinement [66].

The bottleneck limiting the expressiveness of MPNNs is the implicit need to perform graph isomorphism checking, which is challenging in the general case. However, there are well-known classes of graphs, such as planar graphs, with efficient and complete isomorphism algorithms, thus eliminating this bottleneck. For planar graphs, the first complete algorithm for isomorphism testing was presented by Datta et al. [17], Eppstein [20], Hopcroft and Wong [29], and was followed up by a series of algorithms [10, 12, 29, 52]. Kukluk et al. [41] presented an algorithm, which we refer to as KHC, that is more suitable for practical applications, and that we align with in our work. As a result of

this alignment, our approach is the first efficient and complete learning algorithm on planar graphs. The only other complete models on planar graphs are higher-order GNNs with 3-WL (or, *oblivious* 4-WL) power, since 3-WL is complete on planar graphs [38]. However, these models are not scalable in practice, since a  $k$ -WL algorithm computes a  $k$ -stable coloring of an  $n$ -node graph in time  $O(k^2 n^{k+1} \log n)$  [35]. By contrast, our architecture learns representations of efficiently computed components and uses these to obtain refined representations. Our approach extends the inductive biases of MPNNs and introduces structures recently noted to be beneficial in the literature [65].

## 4 A practical planar isomorphism algorithm

We consider simple and undirected planar graphs. The idea behind the KHC algorithm is to compute a canonical code for planar graphs, allowing us to reduce the problem of isomorphism testing to checking whether the codes of the respective graphs are equal. A code can be thought of as a string over  $\Sigma \cup \mathbb{N}$ , where for each graph, the KHC algorithm computes codes for various components resulting from decompositions, and gradually builds a code representation for the graph. For readability, we allow reserved symbols "(", ")", " and ", " in the generated codes. We present an overview of KHC and refer to Kukluk et al. [41] for details. We can assume that the planar graphs are connected, as the algorithm can be extended to disconnected graphs by independently computing the codes for each of the components, and then concatenating them in their lexicographical order.

**Generating a code for the the graph.** Given a connected planar graph  $G = (V, E, \zeta)$ , KHC decomposes  $G$  into a Block-Cut tree  $\delta = \text{BLOCKCUT}(G)$ . Every node  $u \in \delta$  is either a cut node of  $G$ , or a virtual node associated with a biconnected component of  $G$ . KHC iteratively removes the leave nodes of  $\delta$  as follows: if  $u$  is a leaf node associated with a biconnected component  $B$ , KHC uses a subprocedure `BICODE` to compute the canonical code  $\text{CODE}(\delta_u) = \text{BICODE}(B)$  and removes  $u$  from the tree; otherwise, if the leaf node  $u$  is a cut node, KHC overrides the initial code  $\text{CODE}(\{u\}, \{\})$ , using an aggregate code of the removed biconnected components in which  $u$  occurs as a node. This procedure continues until there is a single node left, and the code for this remaining node is taken as the code of the entire connected graph. This process yields a complete graph invariant. Conceptually, it is more convenient for our purposes to reformulate this procedure as follows: we first canonically root  $\delta$ , and then code the subtrees in a *bottom-up procedure*. Specifically, we iteratively generate codes for subtrees and the final code for  $G$  is then simply the code of  $\delta_{\text{root}(\delta)}$ .

**Generating a code for biconnected components.** KHC relies on a subprocedure `BICODE` to compute a code, given a biconnected planar graph  $B$ . Specifically, it uses the SPQR tree  $\gamma = \text{SPQR}(B)$  which uniquely decomposes a biconnected component into a tree with virtual nodes of one of four types:  $S$  for cycle graphs,  $P$  for *two-node dipole* graphs,  $Q$  for a graph that has a *single edge*, and finally  $R$  for a triconnected component that is *not* a dipole or a cycle. We first generate codes for the induced sub-graphs based on these virtual nodes. Then the SPQR tree is canonically rooted, and similarly to the procedure on the Block-Cut tree, we iteratively build codes for the subtrees of  $\gamma$  in a bottom-up fashion. Due to the simpler structure of the SPQR tree, instead of making overrides, the recursive code generation is done by prepending a number  $\theta(C, C')$  for a parent SPQR tree node  $C$  and each  $C' \in \chi(C)$ . This number is generated based on the way  $C$  and  $C'$  are connected in  $B$ . Generating codes for the virtual  $P$  and  $Q$  nodes is trivial. For  $S$  nodes, we use the lexicographically smallest ordering of the cycle, and concatenate the individual node codes. However, for  $R$  nodes we require a more complex procedure and this is done using Weinberg’s algorithm as a subroutine.

**Generating a code for triconnected components.** Whitney [59] has shown that triconnected graphs have only two planar embeddings, and Weinberg introduced an algorithm that computes a canonical code for triconnected planar graphs [57] which we call `TRICODE`. This code is used as one of the building blocks of the KHC algorithm and can be extended to labeled triconnected planar graphs, which is essential for our purposes. Weinberg’s algorithm [57] generates a canonical order for a triconnected component  $T$ , by traversing all the edges in both directions via a walk. Let  $\omega$  be the sequence of visited nodes in this particular walk and write  $\omega[i]$  to denote  $i$ -th node in it. This walk is then used to generate a sequence  $\kappa$  of same length, that corresponds to the order in which we first visit the nodes: for each node  $u = \omega[i]$  that occurs in the walk, we set  $\kappa[i] = 1 + |\{\kappa[j] \mid j < i\}|$  if  $\omega[i]$  is the first occurrence of  $u$ , or  $\kappa[i] = \kappa[\min\{j \mid \omega[j] = \omega[i]\}]$  otherwise. For example, the walk  $\omega = \langle v_1, v_3, v_2, v_3, v_1 \rangle$  yields  $\kappa = \langle 1, 2, 3, 2, 1 \rangle$ . Given such a walk of length  $k$  and a corresponding sequence  $\kappa$ , we compute the following canonical code:  $\text{TRICODE}(T) = (\kappa[1], \text{CODE}(\{\omega[1]\}, \{\})), \dots, (\kappa[k], \text{CODE}(\{\omega[k]\}, \{\}))$ .

## 5 PLANE: Representation learning over planar graphs

KHC generates a unique code for every planar graph in a hierarchical manner based on the decompositions. Our framework aligns with this algorithm: we learn representations for nodes, the respective components, and the graph. Given a planar graph  $G = (V, E, \zeta)$ , PLANE sets the initial node representations  $\mathbf{h}_u^{(0)} = \zeta(u)$  for each node  $u \in V$ , and computes, for every layer  $1 \leq \ell \leq L$ , the representations  $\mathbf{h}_C^{(\ell)}$  of components of  $\sigma^G$ , the representations  $\mathbf{h}_B^{(\ell)}$  of biconnected components  $B \in \pi^G$ , the representations  $\mathbf{h}_{\delta_u}^{(\ell)}$  of subtrees in the Block-Cut tree  $\delta = \text{BLOCKCUT}(G)$  for each node  $u \in V$ , and the representations  $\mathbf{h}_u^{(\ell)}$  of nodes as:

$$\begin{aligned} \mathbf{h}_C^{(\ell)} &= \text{TRIENC}(C, \{(\mathbf{h}_u^{(\ell-1)}, u) \mid u \in C\}) \\ \mathbf{h}_B^{(\ell)} &= \text{BIENC}(B, \{(\mathbf{h}_C^{(\ell)}, C) \mid C \in \sigma^B\}) \\ \mathbf{h}_{\delta_u}^{(\ell)} &= \text{CUTENC}(\delta_u, \{(\mathbf{h}_v^{(\ell-1)}, v) \mid v \in V\}, \{(\mathbf{h}_B^{(\ell)}, B) \mid B \in \pi^G\}) \\ \mathbf{h}_u^{(\ell)} &= \phi(\mathbf{h}_u^{(\ell-1)}, \{\{\mathbf{h}_v^{(\ell-1)} \mid v \in N_u\}, \{\{\mathbf{h}_v^{(\ell-1)} \mid v \in V\}, \{\{\mathbf{h}_T^{(\ell)} \mid T \in \sigma_u^G\}, \{\{\mathbf{h}_B^{(\ell)} \mid B \in \pi_u^G\}, \mathbf{h}_{\delta_u}^{(\ell)}\}) \end{aligned}$$

where TRIENC, BIENC, and CUTENC are invariant encoders; and  $\phi$  is an UPDATE function. The encoders TRIENC and BIENC are parallel to the code generation procedures TRICODE and BICODE of the KHC algorithm. Since PLANE operates by learning node representations, we further simplify the final graph code generation, by learning embeddings for the cut nodes, which is implemented by the CUTENC encoder. For graph-level tasks, we apply a *pooling* function on final node embeddings, mapping the multiset of final node embeddings to a graph-level embedding which is denoted as  $\mathbf{z}_G^{(L)}$ .

There are many choices for deriving PLANE architectures, but we propose a simple model, BASE-PLANE, to clearly identify the virtue of the model architecture which aligns with KHC, as follows:

**TRIENC.** Given a component  $C$  and the previous node representations  $\mathbf{h}_u^{(\ell-1)}$  of each node  $u$ , TRIENC encodes  $C$  based on the walk  $\omega$  given by Weinberg’s algorithm, and its corresponding sequence  $\kappa$  as:

$$\mathbf{h}_C^{(\ell)} = \text{MLP} \left( \sum_{i=1}^{|\omega|} \text{MLP} \left( \mathbf{h}_{\omega[i]}^{(\ell-1)} \parallel \mathbf{p}_{\kappa[i]} \parallel \mathbf{p}_i \right) \right),$$

where  $\mathbf{p}_x \in \mathbb{R}^d$  is the positional embedding [56]. This is a simple sequence model with a positional encoding on the walk, and a second one based on the generated sequence  $\kappa$ . Edge features can also be concatenated while respecting the edge order given by the walk. The nodes of  $\text{SPQR}(G)$  are one of the types  $S, P, Q, R$ , where for  $S, P, Q$  types, we have a trivial ordering for the induced components, and Weinberg’s algorithm also gives an ordering for  $R$  nodes that correspond to triconnected components.

**BIENC.** Given a biconnected component  $B$  and the representations  $\mathbf{h}_C^{(\ell)}$  of each component induced by a node  $C$  in  $\gamma = \text{SPQR}(B)$ , BIENC uses the SPQR tree and the integers  $\theta(C, C')$  corresponding to how we connect  $C$  and  $C' \in \chi(C)$ . BIENC then computes a representation for each subtree  $\gamma_C$  induced by a node  $C$  in a bottom up fashion as:

$$\mathbf{h}_{\gamma_C}^{(\ell)} = \text{MLP} \left( \mathbf{h}_C^{(\ell)} + \sum_{C' \in \chi(C)} \text{MLP} \left( \mathbf{h}_{\gamma_{C'}}^{(\ell)} \parallel \mathbf{p}_{\theta(C, C')} \right) \right).$$

This encoder operates in a bottom up fashion to ensure that a subtree representation of the children of  $C$  exists before it encodes the subtree  $\gamma_C$ . The representation of the canonical root node in  $\gamma$  is used as the representation of the biconnected component  $B$  by setting:  $\mathbf{h}_B^{(\ell)} = \mathbf{h}_{\gamma_{\text{root}(\gamma)}}$ .

**CUTENC.** Given a subtree  $\delta_u$  of a Block-Cut tree  $\delta$ , the representations  $\mathbf{h}_B^{(\ell)}$  of each biconnected component  $B$ , and the node representations  $\mathbf{h}_u^{(\ell-1)}$  of each node, CUTENC sets  $\mathbf{h}_{\delta_u}^{(\ell)} = \mathbf{0}^{d(\ell)}$  if  $u$  is *not* a cut node; otherwise, it computes the subtree representations as:

$$\mathbf{h}_{\delta_u}^{(\ell)} = \text{MLP} \left( \mathbf{h}_u^{(\ell-1)} + \sum_{B \in \chi(u)} \text{MLP} \left( \mathbf{h}_B^{(\ell)} + \sum_{v \in \chi(B)} \mathbf{h}_{\delta_v}^{(\ell)} \right) \right).$$

The CUTENC procedure is called in a bottom-up order to ensure that the representations of the grandchildren are already computed. We learn the cut node subtree representations instead of employing the hierarchical overrides that are present in the KHC algorithm, as the latter is not ideal in a learning algorithm. However, with sufficient layers, these representations are complete invariants.

**UPDATE.** Putting these altogether, we update the node representations  $\mathbf{h}_u^{(\ell)}$  of each node  $u$  as:

$$\mathbf{h}_u^{(\ell)} = f^{(\ell)} \left( g_1^{(\ell)} \left( \mathbf{h}_u^{(\ell-1)} + \sum_{v \in N_u} \mathbf{h}_v^{(\ell-1)} \right) \parallel g_2^{(\ell)} \sum_{v \in V} \mathbf{h}_v^{(\ell-1)} \parallel g_3^{(\ell)} \left( \mathbf{h}_u^{(\ell-1)} + \sum_{B \in \pi_u^G} \mathbf{h}_B^{(\ell)} \right) \parallel g_4^{(\ell)} \left( \mathbf{h}_u^{(\ell-1)} + \sum_{C \in \sigma_u^G} \mathbf{h}_C^{(\ell)} \right) \parallel \mathbf{h}_{\delta_u}^{(\ell)} \right),$$

where  $f^{(\ell)}$  and  $g_i^{(\ell)}$  are either linear maps or two-layer MLPs. To obtain a graph-level representation, we pool as follows:

$$\mathbf{z}_G = \text{MLP} \left( \left\| \sum_{u \in V^G} \mathbf{h}_u^{(\ell)} \right\| \right).$$

## 6 Expressive power of BASEPLANE

We present the theoretical result of this paper, which states that BASEPLANE can distinguish any pair of planar graphs, even when using only a logarithmic number of layers in the size of the input graphs:

**Theorem 6.1.** *For any planar graphs  $G_1 = (V_1, E_1, \zeta_1)$  and  $G_2 = (V_2, E_2, \zeta_2)$ , there exists a parametrization of BASEPLANE with at most  $L = \lceil \log_2(\max\{|V_1|, |V_2|\}) \rceil + 1$  layers, which computes a complete graph invariant, that is, the final graph-level embeddings satisfy  $\mathbf{z}_{G_1}^{(L)} \neq \mathbf{z}_{G_2}^{(L)}$  if and only if  $G_1$  and  $G_2$  are not isomorphic.*

The construction is non-uniform, since the number of layers needed depends on the size of the input graphs. In this respect, our result is similar to other results aligning GNNs with 1-WL with sufficiently many layers [45, 62]. There are, however, two key differences: (i) BASEPLANE computes isomorphism-complete invariants over planar graphs and (ii) our construction requires only logarithmic number of layers in the size of the input graphs (as opposed to linear).

The theorem builds on the properties of each encoder being complete. We first show that a single application of TRIENC and BIENC is sufficient to encode all relevant components of an input graph in an isomorphism-complete way:

**Lemma 6.2.** *Let  $G = (V, E, \zeta)$  be a planar graph. Then, for any biconnected components  $B, B'$  of  $G$ , and for any SPQR components  $C$  and  $C'$  of  $G$ , there exists a parametrization of the functions TRIENC and BIENC such that:*

- (i)  $\mathbf{h}_B \neq \mathbf{h}_{B'}$ , if and only if  $B$  and  $B'$  are not isomorphic, and
- (ii)  $\mathbf{h}_C \neq \mathbf{h}_{C'}$ , if and only if  $C$  and  $C'$  are not isomorphic.

Intuitively, this result follows from a natural alignment to the procedures of the KHC algorithm: the existence of unique codes for different components is proven for the algorithm and we lift this result to the embeddings of the respective graphs, using the universality of MLPs [15, 31, 32].

Our main result rests on a key result related to CUTENC, which states that BASEPLANE computes complete graph invariants for all subtrees of the Block-Cut tree. We use an inductive proof, where the logarithmic bound stems from a single layer computing complete invariants for all subtrees induced by cut nodes that have at most one grandchild cut node, the induced subtree of which is incomplete.

**Lemma 6.3.** *For a planar graph  $G = (V, E, \zeta)$  of order  $n$  and its associated Block-Cut tree  $\delta = \text{BLOCKCUT}(G)$ , there exists a  $L = \lceil \log_2(n) \rceil + 1$  layer parametrization of BASEPLANE that computes a complete graph invariant for each subtree  $\delta_u$  induced by each cut node  $u$ .*

With Lemma 6.2 and Lemma 6.3 in place, Theorem 6.1 follows from the fact that every biconnected component and every cut node of the graph are encoded in an isomorphism-complete way, which is sufficient for distinguishing planar graphs.

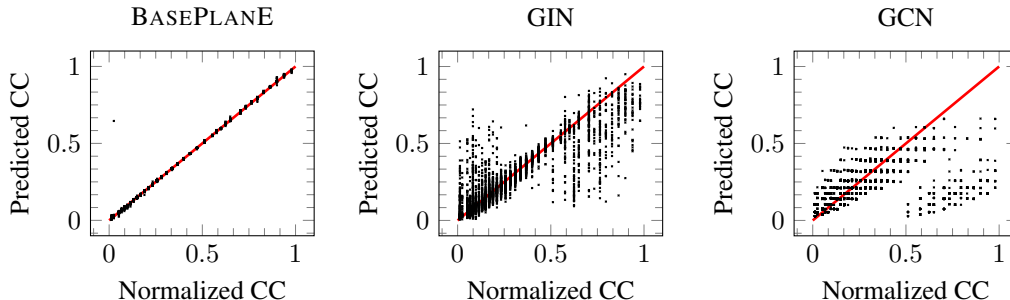


Figure 4: Scatter plots of BASEPLANE, GIN, and GCN predictions versus the true normalized CC. The red line represents ideal behavior where predictions match the true normalized CC.

## 7 Experimental Evaluation

In this section, we evaluate BASEPLANE in three different settings. First, we conduct a synthetic experiment to study the structural inductive bias of BASEPLANE. Second, we evaluate a BASEPLANE variant using edge features on the MolHIV graph classification task from OGB [33, 60]. Finally, we evaluate this variant on graph regression over ZINC [19] and QM9 [13, 48]. We provide hyperparameter grids and training setup, as well as a study of BASEPLANE’s expressive power using EXP [1], and an ablation study on ZINC in the appendix.

### 7.1 Clustering coefficient of QM9 graphs

In this experiment, we evaluate the ability of BASEPLANE to detect structural graph signals *without* an explicit reference to the target structure. To this end, we propose a simple, yet challenging, synthetic task: given a subset of graphs from QM9, we aim to predict the graph-level *clustering coefficient* (CC). Computing CC requires counting triangles in the graph, which is impossible to solve with standard MPNNs [64]. Moreover, triangles are not explicitly extracted in the original planarity algorithm that underpins BASEPLANE, and thus the model must learn to detect triangles.

**Data setup.** We select a subset of graphs from QM9, which we call  $QM9_{CC}$ , to obtain a diverse distribution of CCs. As most QM9 graphs have a CC of 0, we consider graphs with a CC in the interval  $[0.06, 0.16]$ , as this range has high variability. We then normalize the CCs to the unit interval  $[0, 1]$ . We apply the earlier filtering on the original QM9 splits to obtain train/validation/test sets that are direct subsets of the full QM9 splits, and which consist of 44226, 3941 and 3921 graphs, respectively. The overall label distribution in this dataset is depicted in Figure 3.

**Experimental setup.** Given the small size of QM9 and the locality of triangle counting, we use 32-dimensional node embeddings and 3 layers across all models. Moreover, we use a common 100 epoch training setup for fairness. For evaluation, we report mean absolute error (MAE) on the test set, averaged across 5 runs. For this experiment, our baselines are (i) an input-agnostic constant prediction that returns a minimal test MAE, (ii) the MPNNs GCNs [40] and GIN [62], (iii) ESAN [7], an MPNN that computes sub-structures through node and edge removals, but which does *not* explicitly extract triangles, and (iv) BASEPLANE, using 16-dimensional positional encoding vectors.

**Results.** Results on  $QM9_{CC}$  are provided in Table 1. BASEPLANE comfortably outperforms standard MPNNs. Indeed, GCN performance is only marginally better than the constant baseline and GIN’s MAE is over an order of magnitude behind BASEPLANE. This is a very substantial gap, and confirms that MPNNs are unable to accurately detect triangles to compute CCs.

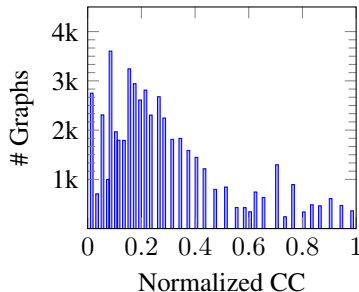


Figure 3: Normalized clustering coefficient distribution of  $QM9_{CC}$ .

Moreover, BASEPLANE achieves an MAE over 40% lower than ESAN. Overall, BASEPLANE effectively detects triangle structures, despite these not being explicitly provided, and thus its underlying algorithmic decomposition effectively captures latent structural graph properties in this setting.

**Performance analysis.** To better understand our results, we visualize the predictions of BASEPLANE, GIN, and GCN using scatter plots in Figure 4. As expected, BASEPLANE essentially follows the ideal regression line. By contrast, GIN and GCN are much less stable. Indeed, GIN struggles with CCs at the extremes of the  $[0, 1]$  range, but is better at intermediate values, whereas GCN is consistently unreliable, and rarely returns predictions above 0.7. This highlights the structural limitation of GCNs, namely its self-loop mechanism for representation updates, which causes ambiguity for detecting triangles.

## 7.2 Graph classification on MolHIV

**Model setup.** We use a BASEPLANE variant that uses edge features, called E-BASEPLANE (defined in the appendix), on OGB [33] MolHIV and compare against baselines. We instantiate E-BASEPLANE with an embedding dimension of 64, 16-dimensional positional encodings, and report the average ROC-AUC across 10 independent runs.

**Results.** The results for E-BASEPLANE and other baselines on MolHIV are shown in Table 2: Despite not explicitly extracting relevant cycles and/or molecular sub-structures, E-BASEPLANE outperforms standard MPNNs and the domain-specific HIMP model. It is also competitive with substructure-aware models CIN and GSN, which include dedicated structures for inference. Therefore, E-BASEPLANE performs strongly in practice with minimal design effort, and effectively uses its structural inductive bias to remain competitive with dedicated architectures.

## 7.3 Graph regression on QM9

**Experimental setup.** We map QM9 [48] edge types into features by defining a learnable embedding per edge type, and subsequently apply E-BASEPLANE to the dataset. We evaluate E-BASEPLANE on all 13 QM9 properties following the same splits and protocol (with MAE results averaged over 5 test set reruns) of GNN-FiLM [13]. We compare R-SPN against GNN-FiLM models and their fully adjacent (FA) variants [3], as well as shortest path networks (SPNs) [2]. We report results with an 3-layer E-BASEPLANE using 128-dimensional node embeddings and 32-dimensional positional encodings.

**Results.** E-BASEPLANE results on QM9 are provided in Table 3. In this table, E-BASEPLANE outperforms high-hop SPNs, despite being simpler and more efficient, achieving state-of-the-art results on 9 of the 13 tasks. The gains are particularly prominent on the first five properties, where R-SPNs originally provided relatively little improvement over FA models, suggesting that E-BASEPLANE offers complementary structural advantages to SPNs. This was corroborated in our experimental tuning: E-BASEPLANE performance peaks around 3 layers, whereas SPN performance continues to improve up to 8 (and potentially more) layers, which suggests that E-BASEPLANE is more efficient at directly communicating information, making further message passing redundant.

Overall, E-BASEPLANE maintains the performance levels of R-SPN with a smaller computational footprint. Indeed, messages for component representations efficiently propagate over trees in E-BASEPLANE, and the number of added components is small (see appendix for more details). Therefore E-BASEPLANE and the PLANE framework offer a more scalable alternative to explicit higher-hop neighborhood message passing over planar graphs.

Table 1: MAE of BASEPLANE and baselines on the QM9<sub>CC</sub> dataset.

Model	MAE
Constant	0.1627 $\pm$ 0.0000
GCN	0.1275 $\pm$ 0.0012
GIN	0.0612 $\pm$ 0.0018
ESAN	0.0038 $\pm$ 0.0010
BASEPLANE	<b>0.0023</b> $\pm$ 0.0004

Table 2: ROC-AUC of BASEPLANE and baselines on MolHIV.

GCN [40]	75.58 $\pm$ 0.97
GIN [62]	77.07 $\pm$ 1.40
PNA [14]	79.05 $\pm$ 1.32
ESAN [7]	78.00 $\pm$ 1.42
GSN [11]	80.39 $\pm$ 0.90
CIN [9]	<b>80.94</b> $\pm$ 0.57
HIMP [21]	78.80 $\pm$ 0.82
E-BASEPLANE	80.04 $\pm$ 0.50



Table 3: MAE of E-BASEPLANE and baselines on QM9. Other model results and their fully adjacent (FA) extensions are as previously reported [2, 3].

Property	R-GIN		R-GAT		R-SPN		BASEPLANE
	base	+FA	base	+FA	$k = 5$	$k = 10$	
mu	2.64±0.11	2.54±0.09	2.68±0.11	2.73±0.07	2.16±0.08	2.21±0.21	<b>1.97</b> ±0.03
alpha	4.67±0.52	2.28±0.04	4.65±0.44	2.32±0.16	1.74±0.05	1.66±0.06	<b>1.63</b> ±0.01
HOMO	1.42±0.01	1.26±0.02	1.48±0.03	1.43±0.02	1.19±0.04	1.20±0.08	<b>1.15</b> ±0.01
LUMO	1.50±0.09	1.34±0.04	1.53±0.07	1.41±0.03	1.13±0.01	1.20±0.06	<b>1.06</b> ±0.02
gap	2.27±0.09	1.96±0.04	2.31±0.06	2.08±0.05	1.76±0.03	1.77±0.06	<b>1.73</b> ±0.02
R2	15.63±1.40	12.61±0.37	52.39±42.5	15.76±1.17	10.59±0.35	10.63±1.01	<b>10.53</b> ±0.55
ZPVE	12.93±1.81	5.03±0.36	14.87±2.88	5.98±0.43	3.16±0.06	2.58±0.13	2.81±0.16
U0	5.88±1.01	2.21±0.12	7.61±0.46	2.19±0.25	1.10±0.03	0.89±0.05	0.95±0.04
U	18.71±23.36	2.32±0.18	6.86±0.53	2.11±0.10	1.09±0.05	0.93±0.03	0.94±0.04
H	5.62±0.81	2.26±0.19	7.64±0.92	2.27±0.29	1.10±0.03	0.92±0.03	0.92±0.04
G	5.38±0.75	2.04±0.24	6.54±0.36	2.07±0.07	1.04±0.04	0.83±0.05	0.88±0.04
Cv	3.53±0.37	1.86±0.03	4.11±0.27	2.03±0.14	1.34±0.03	1.23±0.06	<b>1.20</b> ±0.06
Omega	1.05±0.11	0.80±0.04	1.48±0.87	0.73±0.04	0.53±0.02	0.52±0.02	<b>0.45</b> ±0.01

## 7.4 Graph regression on ZINC

**Experimental setup.** We (i) evaluate BASEPLANE on the ZINC subset (12k graphs) without edge features, (ii) evaluate E-BASEPLANE on this subset and on the full ZINC dataset (500k graphs). To this end, we run BASEPLANE and E-BASEPLANE with 64 and 128-dimensional embeddings, 16-dimensional positional embeddings, and 3 layers. For evaluation, we compute MAE on the respective test sets, and report the best average of 10 runs across all experiments.

**Results.** Results on ZINC are shown in Table 4: Both BASEPLANE and E-BASEPLANE perform strongly, with E-BASEPLANE achieving state-of-the-art performance on ZINC12k with edge features and both models outperforming all but one baseline in the other two settings. These results are very promising, and highlight the robustness of (E-)BASEPLANE.

Table 4: MAE of (E-)BASEPLANE and baselines on ZINC.

Edge Features	ZINC(12k)	ZINC(12k)	ZINC(Full)
	No	Yes	Yes
GCN [40]	0.278±0.003	-	-
GIN(-E) [34, 62]	0.387±0.015	0.252±0.014	0.088±0.002
PNA [14]	0.320±0.032	0.188±0.004	0.320±0.032
GSN [11]	0.140±0.006	0.101±0.010	-
CIN [9]	<b>0.115</b> ±0.003	0.079±0.006	<b>0.022</b> ±0.002
ESAN [7]	-	0.102±0.003	-
HIMP [21]	-	0.151±0.006	0.036±0.002
(E-)BASEPLANE	0.124±0.004	<b>0.076</b> ±0.003	0.028±0.002

## 8 Limitations, discussions, and outlook

Overall, both BASEPLANE and E-BASEPLANE perform strongly across all our experimental evaluation tasks, despite competing against specialized models in each setting. Moreover, both models belong to the PLANE framework, and thus are isomorphism-complete over planar graphs. This implies that these models benefit substantially from the structural inductive bias and expressiveness of classical planar algorithms, which in turn makes them a reliable, efficient, and robust solution for graph representation learning over planar graphs.

Though the PLANE framework is a highly effective and easy to use solution for planar graph representation learning, it is currently limited to planar graphs. Indeed, the classical algorithms underpinning PLANE do not naturally extend beyond the planar graph setting, which in turn limits the applicability of the approach. Thus, a very important avenue for future work is to explore alternative (potentially incomplete) graph decompositions that strike a balance between structural inductive bias, efficiency and expressiveness on more general classes of graphs.

## Acknowledgments and Disclosure of Funding

The authors would like to acknowledge the use of the University of Oxford Advanced Research Computing (ARC) facility in carrying out this work. (<http://dx.doi.org/10.5281/zenodo.22558>)

## References

- [1] Ralph Abboud, İsmail İlkan Ceylan, Martin Grohe, and Thomas Lukasiewicz. The surprising power of graph neural networks with random node initialization. In *Proceedings of the Thirtieth International Joint Conference on Artificial Intelligence, IJCAI*, 2021.
- [2] Ralph Abboud, Radoslav Dimitrov, and İsmail İlkan Ceylan. Shortest path networks for graph property prediction. In *Proceedings of the First Annual Learning on Graphs Conference, LoG*, volume 198 of *Proceedings of Machine Learning Research*, page 5. PMLR, 2022.
- [3] Uri Alon and Eran Yahav. On the bottleneck of graph neural networks and its practical implications. In *Proceedings of the Ninth International Conference on Learning Representations, ICLR*, 2021.
- [4] László Babai. Graph isomorphism in quasipolynomial time. *CoRR*, abs/1512.03547, 2015.
- [5] Pablo Barceló, Egor V. Kostylev, Mikaël Monet, Jorge Pérez, Juan L. Reutter, and Juan Pablo Silva. The logical expressiveness of graph neural networks. In *Proceedings of the Eighth International Conference on Learning Representations, ICLR*, 2020.
- [6] Peter W. Battaglia, Jessica B. Hamrick, Victor Bapst, Alvaro Sanchez-Gonzalez, Vinícius Flores Zambaldi, Mateusz Malinowski, Andrea Tacchetti, David Raposo, Adam Santoro, Ryan Faulkner, Çağlar Gülçehre, H. Francis Song, Andrew J. Ballard, Justin Gilmer, George E. Dahl, Ashish Vaswani, Kelsey R. Allen, Charles Nash, Victoria Langston, Chris Dyer, Nicolas Heess, Daan Wierstra, Pushmeet Kohli, Matthew Botvinick, Oriol Vinyals, Yujia Li, and Razvan Pascanu. Relational inductive biases, deep learning, and graph networks. *CoRR*, abs/1806.01261, 2018.
- [7] Beatrice Bevilacqua, Fabrizio Frasca, Derek Lim, Balasubramaniam Srinivasan, Chen Cai, Gopinath Balamurugan, Michael M. Bronstein, and Haggai Maron. Equivariant subgraph aggregation networks. In *Proceedings of the Tenth International Conference on Learning Representations, ICLR*, 2022.
- [8] Sandeep N Bhatt and Frank Thomson Leighton. A framework for solving vlsi graph layout problems. *Journal of Computer and System Sciences*, 28(2):300–343, 1984.
- [9] Cristian Bodnar, Fabrizio Frasca, Nina Otter, Yuguang Wang, Pietro Liò, Guido F. Montúfar, and Michael M. Bronstein. Weisfeiler and leman go cellular: CW networks. In Marc’Aurelio Ranzato, Alina Beygelzimer, Yann N. Dauphin, Percy Liang, and Jennifer Wortman Vaughan, editors, *Proceedings of the Thirty-Fourth Annual Conference on Advances in Neural Information Processing Systems, NeurIPS*, pages 2625–2640, 2021.
- [10] Kellogg S Booth and George S Lueker. Testing for the consecutive ones property, interval graphs, and graph planarity using pq-tree algorithms. *Journal of Computer and System Sciences*, 13(3):335–379, 1976.
- [11] Giorgos Bouritsas, Fabrizio Frasca, Stefanos Zafeiriou, and Michael M. Bronstein. Improving graph neural network expressivity via subgraph isomorphism counting. *IEEE Transactions on Pattern Analysis and Machine Intelligence*, 45(1):657–668, 2023.
- [12] John M. Boyer and Wendy J. Myrvold. On the cutting edge: Simplified  $O(n)$  planarity by edge addition. *Journal of Graph Algorithms and Applications*, 8(3):241–273, 2004.
- [13] Marc Brockschmidt. GNN-FiLM: Graph neural networks with feature-wise linear modulation. In *Proceedings of the Thirty-Seventh International Conference on Machine Learning, ICML*, pages 1144–1152, 2020.

- [14] Gabriele Corso, Luca Cavalleri, Dominique Beaini, Pietro Liò, and Petar Velickovic. Principal neighbourhood aggregation for graph nets. In Hugo Larochelle, Marc’ Aurelio Ranzato, Raia Hadsell, Maria-Florina Balcan, and Hsuan-Tien Lin, editors, *Proceedings of the Thirty-Third Annual Conference on Advances in Neural Information Processing Systems, NeurIPS*, pages 13260–13271, 2020.
- [15] George Cybenko. Approximation by superpositions of a sigmoidal function. *Mathematics of Control, Signals and Systems*, 2(4):303–314, 1989.
- [16] George Dasoulas, Ludovic Dos Santos, Kevin Scaman, and Aladin Virmaux. Coloring graph neural networks for node disambiguation. In *Proceedings of the Twenty-Ninth International Joint Conference on Artificial Intelligence, IJCAI*, 2020.
- [17] Samir Datta, Nutan Limaye, Prajakta Nimbhorkar, Thomas Thierauf, and Fabian Wagner. Planar graph isomorphism is in log-space. In *2009 24th Annual IEEE Conference on Computational Complexity*, pages 203–214. IEEE, 2009.
- [18] David Duvenaud, Dougal Maclaurin, Jorge Aguilera-Iparraguirre, Rafael Gómez-Bombarelli, Timothy Hirzel, Alán Aspuru-Guzik, and Ryan P. Adams. Convolutional networks on graphs for learning molecular fingerprints. In *Proceedings of the Twenty-Eighth Annual Conference on Advances in Neural Information Processing Systems, NIPS*, pages 2224–2232, 2015.
- [19] Vijay Prakash Dwivedi, Chaitanya K. Joshi, Anh Tuan Luu, Thomas Laurent, Yoshua Bengio, and Xavier Bresson. Benchmarking graph neural networks. *Journal of Machine Learning Research*, 24:43:1–43:48, 2023.
- [20] David Eppstein. Subgraph isomorphism in planar graphs and related problems. In *Graph Algorithms and Applications I*, pages 283–309. World Scientific, 2002.
- [21] Matthias Fey, Jan-Gin Yuen, and Frank Weichert. Hierarchical inter-message passing for learning on molecular graphs. *CoRR*, abs/2006.12179, 2020. URL <https://arxiv.org/abs/2006.12179>.
- [22] Alex Fout, Jonathon Byrd, Basir Shariat, and Asa Ben-Hur. Protein interface prediction using graph convolutional networks. In *Proceedings of the Thirtieth Annual Conference on Advances in Neural Information Processing Systems, NIPS*, pages 6530–6539, 2017.
- [23] Justin Gilmer, Samuel S. Schoenholz, Patrick F. Riley, Oriol Vinyals, and George E. Dahl. Neural message passing for quantum chemistry. In *Proceedings of the Thirty-Fourth International Conference on Machine Learning, ICML*, pages 1263–1272, 2017.
- [24] Marco Gori, Gabriele Monfardini, and Franco Scarselli. A new model for learning in graph domains. In *Proceedings of the 2005 IEEE International Joint Conference on Neural Networks, IJCNN*, volume 2, pages 729–734, 2005.
- [25] Martin Grohe. *Descriptive Complexity, Canonisation, and Definable Graph Structure Theory*. Lecture Notes in Logic. Cambridge University Press, 2017. doi: 10.1017/9781139028868.
- [26] Martin Grohe. The logic of graph neural networks. In *Proceedings of the 36th Annual ACM/IEEE Symposium on Logic in Computer Science, LICS*, New York, NY, USA, 2021. Association for Computing Machinery.
- [27] Martin Grohe and Pascal Schweitzer. The graph isomorphism problem. *Communications of the ACM*, 63(11):128–134, 2020.
- [28] Carsten Gutwenger and Petra Mutzel. A linear time implementation of SPQR-trees. *LNCS*, 1984, 09 2000.
- [29] J. E. Hopcroft and J. K. Wong. Linear time algorithm for isomorphism of planar graphs (preliminary report). In *Proceedings of the Sixth Annual ACM Symposium on Theory of Computing, STOC ’74*, page 172–184. Association for Computing Machinery, 1974.
- [30] John Hopcroft and Robert Tarjan. A v2 algorithm for determining isomorphism of planar graphs. *Information Processing Letters*, 1(1):32–34, 1971.

- [31] Kurt Hornik. Approximation capabilities of multilayer feedforward networks. *Neural Networks*, 4(2):251–257, 1991.
- [32] Kurt Hornik, Maxwell Stinchcombe, and Halbert White. Multilayer feedforward networks are universal approximators. *Neural Networks*, 2(5):359–366, 1989.
- [33] Weihua Hu, Matthias Fey, Marinka Zitnik, Yuxiao Dong, Hongyu Ren, Bowen Liu, Michele Catasta, and Jure Leskovec. Open graph benchmark: Datasets for machine learning on graphs. In *Proceedings of the Thirty-Third Annual Conference on Advances in Neural Information Processing Systems, NeurIPS*, pages 22118–22133, 2020.
- [34] Weihua Hu, Bowen Liu, Joseph Gomes, Marinka Zitnik, Percy Liang, Vijay S. Pande, and Jure Leskovec. Strategies for pre-training graph neural networks. In *Proceedings of the Eighth International Conference on Learning Representations, ICLR*, 2020.
- [35] Neil Immerman and Eric Lander. *Describing Graphs: A First-Order Approach to Graph Canonization*, pages 59–81. Springer, 1990.
- [36] Steven M. Kearnes, Kevin McCloskey, Marc Berndl, Vijay S. Pande, and Patrick Riley. Molecular graph convolutions: moving beyond fingerprints. *Journal of Computer Aided Molecular Design*, 30(8):595–608, 2016.
- [37] Nicolas Keriven and Gabriel Peyré. Universal invariant and equivariant graph neural networks. In *Proceedings of the Thirty-Second Annual Conference on Advances in Neural Information Processing Systems, NeurIPS*, pages 7090–7099, 2019.
- [38] Sandra Kiefer, Iliia Ponomarenko, and Pascal Schweitzer. The weisfeiler-leman dimension of planar graphs is at most 3. *Journal of the ACM*, 66(6):44:1–44:31, 2019.
- [39] Diederik Kingma and Jimmy Ba. Adam: A method for stochastic optimization. In *Proceedings of the Third International Conference on Learning Representations, ICLR*, 2015.
- [40] Thomas Kipf and Max Welling. Semi-supervised classification with graph convolutional networks. In *Proceedings of the Fifth International Conference on Learning Representations, ICLR*, 2017.
- [41] Jacek P. Kukluk, Lawrence B. Holder, and Diane J. Cook. Algorithm and experiments in testing planar graphs for isomorphism. *Journal of Graph Algorithms and Applications*, 8(3):313–356, 2004.
- [42] Andreas Loukas. What graph neural networks cannot learn: depth vs width. In *Proceedings of the Eighth International Conference on Learning Representations, ICLR*, 2020.
- [43] Haggai Maron, Heli Ben-Hamu, Hadar Serviansky, and Yaron Lipman. Provably powerful graph networks. In *Proceedings of the Thirty-Second Annual Conference on Advances in Neural Information Processing Systems, NeurIPS*, pages 2153–2164, 2019.
- [44] Haggai Maron, Ethan Fetaya, Nimrod Segol, and Yaron Lipman. On the universality of invariant networks. In *Proceedings of the Thirty-Sixth International Conference on Machine Learning, ICML*, pages 4363–4371, 2019.
- [45] Christopher Morris, Martin Ritzert, Matthias Fey, William L. Hamilton, Jan Eric Lenssen, Gaurav Rattan, and Martin Grohe. Weisfeiler and Leman go neural: Higher-order graph neural networks. In *Proceedings of the Thirty-Third AAAI Conference on Artificial Intelligence, AAAI*, pages 4602–4609, 2019.
- [46] Giannis Nikolentzos and Michalis Vazirgiannis. Random walk graph neural networks. In *Proceedings of the Thirty-Third Annual Conference on Advances in Neural Information Processing Systems, NeurIPS*, pages 16211–16222, 2020.
- [47] Bryan Perozzi, Rami Al-Rfou, and Steven Skiena. Deepwalk: online learning of social representations. In *The 20th ACM SIGKDD International Conference on Knowledge Discovery and Data Mining, KDD*, pages 701–710, 2014.

- [48] Raghunathan Ramakrishnan, Pavlo O Dral, Matthias Rupp, and O Anatole Von Lilienfeld. Quantum chemistry structures and properties of 134 kilo molecules. *Scientific data*, 1(1):1–7, 2014.
- [49] Louis C. Ray and Russell A. Kirsch. Finding chemical records by digital computers. *Science*, 126(3278):814–819, 1957.
- [50] Ryoma Sato, Makoto Yamada, and Hisashi Kashima. Random features strengthen graph neural networks. In *Proceedings of the 2021 SIAM International Conference on Data Mining, SDM*, pages 333–341, 2021.
- [51] Franco Scarselli, Marco Gori, Ah Chung Tsoi, Markus Hagenbuchner, and Gabriele Monfardini. The graph neural network model. *IEEE Transactions on Neural Networks*, 20(1):61–80, 2009.
- [52] Wei-Kuan Shih and Wen-Lian Hsu. A new planarity test. *Theoretical Computer Science*, 223(1-2):179–191, 1999.
- [53] Jonathan Shlomi, Peter Battaglia, and Jean-Roch Vlimant. Graph neural networks in particle physics. *Machine Learning: Science and Technology*, 2(2):021001, 2021.
- [54] Howard E. Simmons and John E. Maggio. Synthesis of the first topologically non-planar molecule. *Tetrahedron Letters*, 22(4):287–290, 1981.
- [55] Erik H. Thiede, Wenda Zhou, and Risi Kondor. Autobahn: Automorphism-based graph neural nets. In Marc’Aurelio Ranzato, Alina Beygelzimer, Yann N. Dauphin, Percy Liang, and Jennifer Wortman Vaughan, editors, *Proceedings of the Thirty-Fourth Annual Conference on Advances in Neural Information Processing Systems, NeurIPS*, pages 29922–29934, 2021.
- [56] Ashish Vaswani, Noam Shazeer, Niki Parmar, Jakob Uszkoreit, Llion Jones, Aidan N. Gomez, Lukasz Kaiser, and Illia Polosukhin. Attention is all you need. In Isabelle Guyon, Ulrike von Luxburg, Samy Bengio, Hanna M. Wallach, Rob Fergus, S. V. N. Vishwanathan, and Roman Garnett, editors, *Proceedings of the Thirtieth Annual Conference on Advances in Neural Information Processing Systems, NIPS*, pages 5998–6008, 2017.
- [57] Louis Weinberg. A simple and efficient algorithm for determining isomorphism of planar triply connected graphs. *IEEE Transactions on Circuit Theory*, 13:142–148, 1966.
- [58] Boris Weisfeiler and Andrei A Lehman. A reduction of a graph to a canonical form and an algebra arising during this reduction. *Nauchno-Technicheskaya Informatsia*, 2(9):12–16, 1968.
- [59] Hassler Whitney. A set of topological invariants for graphs. *American Journal of Mathematics*, 55(1):231–235, 1933. ISSN 00029327, 10806377. URL <http://www.jstor.org/stable/2371125>.
- [60] Zhenqin Wu, Bharath Ramsundar, Evan N Feinberg, Joseph Gomes, Caleb Geniesse, Aneesh S Pappu, Karl Leswing, and Vijay Pande. Moleculenet: a benchmark for molecular machine learning. *Chemical science*, 9(2):513–530, 2018.
- [61] Feng Xie and David Levinson. Topological evolution of surface transportation networks. *Computers, Environment, and Urban Systems*, 33(3):211–223, 2009.
- [62] Keyulu Xu, Weihua Hu, Jure Leskovec, and Stefanie Jegelka. How powerful are graph neural networks? In *Proceedings of the Seventh Annual Conference on Learning Representations, ICLR*, 2019.
- [63] Chengxuan Ying, Tianle Cai, Shengjie Luo, Shuxin Zheng, Guolin Ke, Di He, Yanming Shen, and Tie-Yan Liu. Do transformers really perform badly for graph representation? In Marc’Aurelio Ranzato, Alina Beygelzimer, Yann N. Dauphin, Percy Liang, and Jennifer Wortman Vaughan, editors, *Proceedings of the Thirty-Fourth Annual Conference on Advances in Neural Information Processing Systems, NeurIPS*, pages 28877–28888, 2021.
- [64] Jiaxuan You, Jonathan M. Gomes-Selman, Rex Ying, and Jure Leskovec. Identity-aware graph neural networks. In *Proceedings of the Thirty-Fifth AAAI Conference on Artificial Intelligence, AAAI*, pages 10737–10745, 2021.

- [65] Bohang Zhang, Shengjie Luo, Liwei Wang, and Di He. Rethinking the expressive power of gnns via graph biconnectivity. In *Proceedings of the Eleventh International Conference on Learning Representations, ICLR, 2023*.
- [66] Muhan Zhang and Pan Li. Nested graph neural networks. In *Proceedings of the Thirty-Fifth Annual Conference on Advances in Neural Information Processing Systems, NeurIPS*, pages 15734–15747, 2021.
- [67] Marinka Zitnik, Monica Agrawal, and Jure Leskovec. Modeling polypharmacy side effects with graph convolutional networks. *Bioinformatics*, 34(13):i457–i466, 2018.

## A Runtime analysis of BASEPLANE

In this section, we study the complexity of the BASEPLANE model. To this end, we analyze the complexity of the decomposition computation, the sizes of the resulting components, and finally the time to run BASEPLANE on these components.

**Computing components of a planar graph.** Given an input graph  $G = (V, E, \zeta)$ , BASEPLANE first computes the SPQR components/SPQR tree, and identifies cut nodes. For this step, we follow a simple  $O(|V|^2)$  procedure, analogously to the computation in the KHC algorithm. Note that this computation only needs to run once, as a pre-processing step. Therefore, this pre-computation does not ultimately affect runtime for model predictions.

**Size and number of computed components.**

1. *Cut nodes:* The number of cut nodes in  $G$  is at most  $|V|$ , and this corresponds to the worst-case when  $G$  is a tree.
2. *Biconnected Components:* The number of biconnected components  $|\pi^G|$  is at most  $|V| - 1$ , also obtained when  $G$  is a tree. This setting also yields a worst-case bound of  $2|V| - 2$  on the total number of nodes across all individual biconnected components.
3. *SQPR components:* As proved by Gutwenger and Mutzel [28], given a biconnected component  $B$ , the number of corresponding SPQR components, as well as their size, is bounded by the number of nodes in  $B$ . The input graph may have multiple biconnected components, whose total size is bounded by  $2|V| - 2$  as described earlier. Thus, we can apply the earlier result from Gutwenger and Mutzel [28] to obtain an analogous bound of  $2|V| - 2$  on the total number of SPQR components.
4. *SPQR trees:* As each SPQR component corresponds to exactly one node in a SPQR tree. The total size of all SPQR trees is upper-bounded by  $2|V| - 2$ .

**Complexity of TRIENC.** TRIENC computes a representation for each SQPR component edge. This number of edges, which we denote by  $e_C$ , is in fact linear in  $V$ : Indeed, following Euler’s theorem for planar graphs ( $|E| \leq 3|V| - 6$ ), the number of edges per SQPR component is linear in its size. Moreover, since the total number of nodes across all SQPR components is upper-bounded by  $2|V| - 2$ , the total number of edges is in  $O(V)$ . Therefore, as each edge representation can be computed in a constant time with an MLP, TRIENC computes all edge representations across all SQPR components in  $O(e_C \cdot d) = O(|V|d^2)$  time, where  $d$  denotes the embedding dimension of the model.

Using the earlier edge representations, TRIENC performs an aggregation into a triconnected component representation by summing the relevant edge representations, and this is done in  $O(e_C d)$ . Then, the sum outputs across all SPQR components are transformed using an MLP, in  $O(|\sigma^G|d^2)$ . Therefore, the overall complexity of TRIENC is  $O((e_C + |\sigma^G|)d^2) = O(|V|d^2)$ .

**Complexity of BIENC.** BIENC recursively encodes nodes in the SPQR tree. Each SPQR node is aggregated once by its parent and an MLP is applied to each node representation once. The total complexity of this call is therefore  $O(|\sigma^G|d^2) = O(|V|d^2)$ .

**Complexity of CUTENC.** A similar complexity of  $O(|V|d^2)$  applies for CUTENC, as CUTENC follows a similar computational pipeline.

**Complexity of node update.** As in standard MLPs, message aggregation runs in  $O(|E|d)$ , and the combine function runs in  $O(|V|d^2)$ . Global readouts can be computed in  $O(|V|d)$ . Aggregating from bi-connected components also involves at most  $O(|V|d)$  messages, as the number of messages corresponds to the total number of bi-connected component nodes, which itself does not exceed  $2|V| - 2$ . The same argument applies to messages from SQPR components: nodes within these components will message their original graph analogs, leading to the same bound. Finally, the cut node messages are trivially linear, i.e.,  $O(|V|)$ , as each node receives exactly one message (no aggregation, no transformation). Overall, this leads to the step computation having a complexity of  $O(|V|d^2)$ .

**Overall complexity** BASEPLANE runs in  $O(|V|d^2)$  time, as this is the asymptotic bound of each of its individual steps. The  $d^2$  term primarily stems from MLP computations, and is not a main hurdle to scalability, as the used embedding dimensionality in our experiments is usually small.

## B Proofs of the statements

In this section, we provide the proofs of the statements from the main paper. Throughout the proofs, we make the standard assumption that the initial node features are from a compact space  $K \subseteq \mathbb{R}^d$ , for some  $d \in \mathbb{N}^+$ . We also often need to canonically map elements of finite sets to the integer domain: given a finite set  $S$ , and any element  $x \in S$  of this set, the function  $\Psi(S, x) : S \rightarrow \{1, \dots, |S|\}$  maps  $x$  to a unique integer index given by some fixed order over the set  $S$ . Furthermore, we also often need to injectively map sets into real numbers, which is given by the following lemma.

**Lemma B.1.** *Given a bounded set  $S$ , there exists an injective map  $g : \mathbb{P}(S) \rightarrow [0, 1]$ .*

*Proof.* For each subset  $M \subseteq S$ , consider the mapping:

$$g(M) = \frac{1}{1 + \sum_{x \in M} \Psi(S, x) |S|^{\Psi(M, x)}},$$

which clearly satisfies  $g(M_1) \neq g(M_2)$  for any  $M_1 \neq M_2 \subseteq S$ .  $\square$

We now provide proofs for Lemma 6.2, Lemma 6.3 which are essential for Theorem 6.1. Let us first prove Lemma 6.2:

**Lemma 6.2.** *Let  $G = (V, E, \zeta)$  be a planar graph. Then, for any biconnected components  $B, B'$  of  $G$ , and for any SPQR components  $C$  and  $C'$  of  $G$ , there exists a parametrization of the functions TRIENC and BIENC such that:*

- (i)  $h_B \neq h_{B'}$  if and only if  $B$  and  $B'$  are not isomorphic, and
- (ii)  $h_C \neq h_{C'}$  if and only if  $C$  and  $C'$  are not isomorphic.

*Proof.* We show this by first giving a parametrization of TRIENC to distinguish all SPQR components, and then use this construction to give a parametrization of BIENC to distinguish all biconnected components. The proof aligns the encoders with the code generation procedure in the KHC algorithm. The parametrization needs only a single layer, so we will drop the superscripts in the node representations and write, e.g.,  $h_u$ , for brevity. The construction yields single-dimensional real-valued vectors, and, for notational convenience, we view the resulting representations as reals.

**Parametrizing TRIENC.** We initialize the node features as  $h_u = \zeta(u)$ , where  $\zeta : V \rightarrow \mathbb{R}^d$ . Given an SPQR component  $C$  and the initial node representations  $h_u$  of each node  $u$ , TRIENC encodes  $C$  based on the walk  $\omega$  given by Weinberg’s algorithm, and its corresponding sequence  $\kappa$  as:

$$h_C = \text{MLP} \left( \sum_{i=1}^{|\omega|} \text{MLP} (h_{\omega[i]} \| p_{\kappa[i]} \| p_i) \right). \quad (1)$$

In other words, we rely on the walks  $\omega$  generated by Weinberg’s algorithm: we create a walk on the triconnected components that visits each edge exactly twice. Let us fix  $n = 4(|V| + |E| + 1)$ , which serves as an upper bound for size of the walks  $\omega$ , and the size of the walk-induced sequence  $\kappa$ .

We show a bijection between the multiset of codes  $\mathcal{F}$  (given by the KHC algorithm), and the multiset of representations  $\mathcal{M}$  (given by TRIENC), where the respective multisets are defined, based on  $G$ , as follows:

- $\mathcal{F} = \{\{\text{CODE}(C) \mid C \in \sigma^G\}\}$ : the multiset of all codes of the SPQR components of  $G$ .
- $\mathcal{M} = \{\{h_C \mid C \in \sigma^G\}\}$ : the multiset of the representations of the SPQR components of  $G$ .

Specifically, we prove the following:

**Claim 1.** *There exists a bijection  $\rho$  between  $\mathcal{F}$  and  $\mathcal{M}$  such that, for any SPQR component  $C$ :*

$$\rho(h_C) = \text{CODE}(C) \text{ and } \rho^{-1}(\text{CODE}(C)) = h_C.$$



Once Claim 1 established, the desired result is immediate, since, using the bijection  $\rho$ , and the completeness of the codes generated by the KHC algorithm, we obtain:

$$\begin{aligned}
& \mathbf{h}_C \neq \mathbf{h}_{C'} \\
& \Leftrightarrow \\
& \rho^{-1}(\text{CODE}(C)) \neq \rho^{-1}(\text{CODE}(C')) \\
& \Leftrightarrow \\
& \text{CODE}(C) \neq \text{CODE}(C') \\
& \Leftrightarrow \\
& C \text{ and } C' \text{ are non-isomorphic.}
\end{aligned}$$

To prove the Claim 1, first note that the canonical code given by Weinberg's algorithm for any component  $C$  has the form:

$$\begin{aligned}
\text{CODE}(C) &= \text{TRICODE}(C) = (\kappa[1], \text{CODE}(\{\{\omega[1]\}, \{\}\})), \dots, (\kappa[k], \text{CODE}(\{\{\omega[k]\}, \{\}\})) \\
&= (\kappa[1], \zeta(\omega[1])), \dots, (\kappa[k], \zeta(\omega[k])). \tag{2}
\end{aligned}$$

There is a trivial bijection between the codes of the form (2) and sets of the following form:

$$S_C = \{(\zeta(\omega[i]), \kappa[i], i) \mid 1 \leq i \leq |\omega|\}, \tag{3}$$

and, as a result, for each component  $C$ , we can refer to the set  $S_C$  that represents this component  $C$  instead of  $\text{CODE}(C)$ . Sets of this form are of bounded size (since the number of walks are bounded in  $C$ ) and each of their elements is from a countable set (since the graph size is bounded). By Lemma B.1 there exists an injective map  $g$  between such sets and the interval  $[0, 1]$ . Since the size of every such set is bounded, and every tuple is from a countable set, we can apply Lemma 5 of Xu et al. [62], and decompose the function  $g$  as:

$$g(S_C) = \phi \left( \sum_{x \in S_C} f(x) \right),$$

for an appropriate choice of  $\phi : \mathbb{R}^d \rightarrow [0, 1]$  and  $f(x) \in \mathbb{R}^d$ . Based on the structure of the elements of  $S_C$ , we can further rewrite this as follows:

$$g(S_C) = \phi \left( \sum_{i=1}^{|\omega|} f((\zeta(\omega[i]), \kappa[i], i)) \right). \tag{4}$$

Observe that this function closely resembles TRIENC (1). More concretely, for any  $\omega$  and  $i$ , we have that  $\zeta(\omega[i]) = \mathbf{h}_{\omega[i]}$ , and, moreover,  $\mathbf{p}_{\kappa[i]}$  and  $\mathbf{p}_i$  are the positional encodings of  $\kappa[i]$ , and  $i$ , respectively. Hence, it is easy to see that there exists a function  $\mu$ , which satisfies, for every  $i$ :

$$((\zeta(\omega[i]), \kappa[i], i) = \mu(\mathbf{h}_{\omega[i]} \parallel \mathbf{p}_{\kappa[i]} \parallel \mathbf{p}_i).$$

This implies the following:

$$\begin{aligned}
g(S_C) &= \phi \left( \sum_{i=1}^{|\omega|} f((\zeta(\omega[i]), \kappa[i], i)) \right) \\
&= \phi \left( \sum_{i=1}^{|\omega|} f(\mu(\mathbf{h}_{\omega[i]} \parallel \mathbf{p}_{\kappa[i]} \parallel \mathbf{p}_i)) \right) \\
&= \phi \left( \sum_{i=1}^{|\omega|} (f \circ \mu)(\mathbf{h}_{\omega[i]} \parallel \mathbf{p}_{\kappa[i]} \parallel \mathbf{p}_i) \right).
\end{aligned}$$

Observe that this function can be parametrized by TRIENC: we apply the universal approximation theorem [15, 31, 32], and encode  $(f \circ \mu)$  with an MLP (i.e., the inner MLP) and similarly encode  $\phi$  with another MLP (i.e., the outer MLP).

This establishes a bijection  $\rho$  between  $\mathcal{F}$  and  $\mathcal{M}$ : for any SPQR component  $C$ , we can injectively map both the code  $\text{CODE}(C)$  (or, equivalently the corresponding set  $S_C$ ) and the representation  $\mathbf{h}_C$  to the same unique value using the function  $g$  as  $\mathbf{h}_C = g(S_C)$ , and we have shown that there exists a parametrization of TRIENC for this target function  $g$ .

**Parametrizing BIENC.** In this case, we are given a biconnected component  $B$  and the representations  $\mathbf{h}_C$  of each component  $C$  from the SPQR tree  $\gamma = \text{SPQR}(B)$ . We consider the representations  $\mathbf{h}_C$  which are a result of the parametrization of TRIENC, described earlier.

BIENC uses the SPQR tree and the integers  $\theta(C, C')$  corresponding to how we connect  $C$  and  $C' \in \chi(C)$ . BIENC then computes a representation for each subtree  $\gamma_C$  induced by a node  $C$  in a bottom up fashion as:

$$\mathbf{h}_{\gamma_C} = \text{MLP} \left( \mathbf{h}_C + \sum_{C' \in \chi(C)} \text{MLP}(\mathbf{h}_{\gamma_{C'}}, \|\mathbf{p}_{\theta(C, C')}\|) \right). \quad (5)$$

This encoder operates in a bottom up fashion to ensure that a subtree representation of the children of  $C$  exists before it encodes the subtree  $\gamma_C$ . The representation of the canonical root node in  $\gamma$  is used as the representation of the biconnected component  $B$  by setting:  $\mathbf{h}_B = \mathbf{h}_{\gamma_{\text{root}(\gamma)}}$ .

To show the result, we first note that the canonical code given by the KHC algorithm also operates in a bottom up fashion on the subtrees of  $\gamma$ . We have two cases:

*Case 1.* For a *leaf node*  $C$  in  $\gamma$ , the code for  $\gamma_C$  is given by  $\text{CODE}(\gamma_C) = \text{TRICODE}(C)$ . This case can be seen as a special case of Case 2 (and we will treat it as such).

*Case 2.* For a *non-leaf node*  $C$ , we concatenate the codes of the subtrees induced by the children of  $C$  in their lexicographical order, by first prepending the integer given by  $\theta$  to each child code. Then, we also prepend the code of the SPQR component  $C$  to this concatenation to get  $\text{CODE}(\gamma_C)$ . More precisely, if the lexicographical ordering of  $\chi(u)$ , based on  $\text{CODE}(\gamma_{C'})$  for a given  $C' \in \chi(C)$  is  $x[1], \dots, x[|\chi(C)|]$ , then the code for  $\gamma_C$  is given by:

$$\text{CODE}(\gamma_C) = (\text{TRICODE}(C), (\theta(C, x[1]), \text{CODE}(\gamma_{x[1]})), \dots, (\theta(C, x[|x|]), \text{CODE}(\gamma_{x[|x|]}))) \quad (6)$$

We show a bijection between the multiset of codes  $\mathcal{F}$  (given by the KHC algorithm), and the multiset of representations  $\mathcal{M}$  (given by BIENC), where the respective multisets are defined, based on  $G$  and the SPQR tree  $\gamma$ , as follows:

- $\mathcal{F} = \{\{\text{CODE}(\gamma_C) \mid C \in \gamma\}\}$ : the multiset of all codes of all the induced SPQR subtrees.
- $\mathcal{M} = \{\{\mathbf{h}_{\gamma_C} \mid C \in \gamma\}\}$ : the multiset of the representations of all the induced SPQR subtrees.

Analogously to the proof of TRIENC, we prove the following claim:

**Claim 2.** *There exists a bijection  $\rho$  between  $\mathcal{F}$  and  $\mathcal{M}$  such that, for any node  $C$  in  $\gamma$ :*

$$\rho(\mathbf{h}_{\gamma_C}) = \text{CODE}(\gamma_C) \text{ and } \rho^{-1}(\text{CODE}(\gamma_C)) = \mathbf{h}_{\gamma_C}$$

Given Claim 2, the result follows, since, using the bijection  $\rho$ , and the completeness of the codes generated by the KHC algorithm, we obtain:

$$\begin{aligned} \mathbf{h}_B &\neq \mathbf{h}_{B'} \\ &\Leftrightarrow \\ \mathbf{h}_{\gamma_{\text{root}(B)}} &\neq \mathbf{h}_{\gamma_{\text{root}(B')}} \\ &\Leftrightarrow \\ \rho^{-1}(\text{CODE}(\text{ROOT}(B))) &\neq \rho^{-1}(\text{CODE}(\text{ROOT}(B'))) \\ &\Leftrightarrow \\ \text{CODE}(\text{ROOT}(B)) &\neq \text{CODE}(\text{ROOT}(B')) \\ &\Leftrightarrow \\ B \text{ and } B' &\text{ are non-isomorphic.} \end{aligned}$$

To prove Claim 2, let us first consider how  $\text{CODE}(\gamma_C)$  is generated. For any node  $C$  in  $\gamma$ , there is a bijection between the codes of the form given in Equation (10) and sets of the following form:

$$S_C = \{\{\text{TRICODE}(C)\}\} \cup \{(\theta(C, C'), \text{CODE}(\gamma_{C'})) \mid C' \in \chi(C)\} \quad (7)$$

Observe that the sets of this form are of bounded size (since the number of children is bounded) and each of their elements is from a countable set (since the graph size is bounded, the different codes that can be generated are also bounded). By Lemma B.1 there exists an injective map  $g$  from such sets to the interval  $[0, 1]$ . Since the size of every such set is bounded, and every tuple is from a countable set, we can apply Lemma 5 of Xu et al. [62], and decompose the function  $g$  as:

$$g(S_C) = \phi \left( \sum_{x \in S} f(x) \right),$$

for an appropriate choice of  $\phi : \mathbb{R}^d \rightarrow [0, 1]$  and  $f(x) \in \mathbb{R}^d$ . Based on the structure of the elements of  $S_C$ , we can further rewrite this as follows:

$$g(S_C) = \phi \left( f(\text{TRICODE}(C)) + \sum_{C' \in \chi(C)} f((\theta(C, C'), \text{CODE}(\gamma_{C'}))) \right). \quad (8)$$

Observe the connection between this function and BIENC (5): for every  $C' \in \chi(C)$ , we have  $\mathbf{h}_{\gamma_{C'}}$  instead of  $\text{CODE}(\gamma_{C'})$ , and, moreover,  $\mathbf{p}_{\theta(C, C')}$  is a positional encoding of  $\theta(C, C')$ . Then, there exists a function  $\mu$  such that:

$$(\theta(C, C'), \text{CODE}(\gamma_{C'})) = \mu(\mathbf{p}_{\theta(C, C')} \parallel \mathbf{h}_{\gamma_{C'}}),$$

provided that the following condition is met:

$$\mathbf{h}_{\gamma_{C'}} = \text{CODE}(\gamma_{C'}) \text{ for any } C' \in \chi(C). \quad (9)$$

Importantly, the choice for  $\mu$  can be the same for all nodes  $C$ . Hence, assuming the condition specified in Equation (9) is met, the function  $g$  can be further decomposed using some function  $f'(x) \in \mathbb{R}^d$  which satisfies:

$$\begin{aligned} g(S_C) &= \phi \left( f(\{\text{TRICODE}(C)\}) + \sum_{C' \in \chi(C)} f((\theta(C, C'), \text{CODE}(\gamma_{C'}))) \right) \\ &= \phi \left( \mathbf{h}_C + \sum_{C' \in \chi(C)} f'(\mu(\mathbf{p}_{\theta(C, C')} \parallel \mathbf{h}_{\gamma_{C'}})) \right) \\ &= \phi \left( \mathbf{h}_C + \sum_{C' \in \chi(C)} (f' \circ \mu)(\mathbf{p}_{\theta(C, C')} \parallel \mathbf{h}_{\gamma_{C'}}) \right). \end{aligned}$$

Observe that this function can be parametrized by BIENC<sup>2</sup> (5): we apply the universal approximation theorem [15, 31, 32], and encode  $(f' \circ \mu)$  with an MLP (i.e., the inner MLP) and similarly encode  $\phi$  with another MLP (i.e., the outer MLP).

To conclude the proof of Claim 2 (and thereby the proof of Lemma 6.2), we need to show the existence of bijection  $\rho$  between  $\mathcal{F}$  and  $\mathcal{M}$  such that, for any node  $C$  in  $\gamma$ :

$$\rho(\mathbf{h}_{\gamma_C}) = \text{CODE}(\gamma_C) \text{ and } \rho^{-1}(\text{CODE}(\gamma_C)) = \mathbf{h}_{\gamma_C}.$$

This can be shown by a straight-forward induction on the structure of the tree  $\gamma$ . For the base case, it suffices to observe that  $C$  is a leaf node, which implies  $\mathbf{h}_{\gamma_C} = \phi(\mathbf{h}_C)$  and  $\text{CODE}(\gamma_C) = \{\text{TRICODE}(C)\}$ . The existence of a bijection is then warranted by Claim 1. For the inductive case, assume that there is a bijection between the induced representations of the children of  $C$  and their codes to ensure that the condition given in Equation (9) is met (which holds since the algorithm operates in a bottom up manner). Using the injectivity of  $g$ , and the fact that all subtree representations (of children) already admit a bijection, we can easily extend this to a bijection on all nodes  $C$  of  $\gamma$ .

We have provided a parametrization of TRIENC and BIENC and proven that they can compute representations which bijectively map to the codes of the KHC algorithm for the respective components, effectively aligning KHC algorithm with our encoders for these components. Given the completeness of the respective procedures in KHC, we conclude that the encoders are also complete in terms of distinguishing the respective components.  $\square$

<sup>2</sup>Note that  $f(\text{TRICODE}(C))$  can be omitted, because TRIENC has an outer MLP, which can incorporate  $f$ .

Having showed that a single layer parametrization of BIENC and TRIENC is sufficient for distinguishing the biconnected and triconnected components, we proceed with the main lemma.

**Lemma 6.3.** *For a planar graph  $G = (V, E, \zeta)$  of order  $n$  and its associated Block-Cut tree  $\delta = \text{BLOCKCUT}(G)$ , there exists a  $L = \lceil \log_2(n) \rceil + 1$  layer parametrization of BASEPLANE that computes a complete graph invariant for each subtree  $\delta_u$  induced by each cut node  $u$ .*

*Proof.* CUTENC recursively computes the representation for induced subtrees  $\delta_u$  from cut nodes  $u$ , where  $\delta = \text{BLOCKCUT}(G)$ . Recall that in Block-Cut trees, the children of a cut node always represent a biconnected component, and the children of a biconnected component always represent a cut node. Therefore, it is natural to give the update formula for a cut node  $u$  in terms of the biconnected component  $B$  represented by  $u$ 's children  $\chi(u)$  and  $B$ 's children  $\chi(B)$ .

$$\mathbf{h}_{\delta_u}^{(\ell)} = \text{MLP} \left( \mathbf{h}_u^{(\ell-1)} + \sum_{B \in \chi(u)} \text{MLP} \left( \mathbf{h}_B^{(\ell)} + \sum_{v \in \chi(B)} \mathbf{h}_{\delta_v}^{(\ell)} \right) \right).$$

To show the result, we first note that the canonical code given by the KHC algorithm also operates in a bottom up fashion on the subtrees of  $\delta$ . We have three cases:

**Case 1.** For a *leaf*  $B$  in  $\delta$ , the code for  $\delta_B$  is given by  $\text{CODE}(\delta_B) = \text{BICODE}(B)$ . This is because the leafs of  $\delta$  are all biconnected components.

**Case 2.** For a *non-leaf* biconnected component  $B$  in  $\delta$ , we perform overrides for the codes associated with each child cut node, and then use BIENC. More precisely, we override the associated  $\text{CODE}(\{\{u\}, \{\}\}) := \text{CODE}(\delta_u)$  for all  $u \in \chi(B)$ , and then we compute  $\text{CODE}(\delta_B) = \text{BICODE}(B)$ .

**Case 3.** For a *non-leaf* cut node  $u$  in  $\delta$ , we encode in a similar way to BIENC: we get the set of codes induced by the children of  $u$  in their lexicographical order. More precisely, if the lexicographical ordering of  $\chi(u)$ , based on  $\text{CODE}(\delta_B)$  for a given  $B \in \chi(u)$  is  $x[1], \dots, x[|\chi(u)|]$ , then the code for  $\delta_u$  is given by:

$$\text{CODE}(\delta_u) = (\text{CODE}(\delta_{x[1]}), \dots, \text{CODE}(\delta_{x[|\chi(u)|]})) \quad (10)$$

Instead of modelling the overrides (as in Case 2), BASEPLANE learns the cut node representations. We first prove this result by giving a parametrization of BASEPLANE which uses linearly many layers in  $n$  and then show how this construction can be improved to use logarithmic number of layers. Specifically, we will first show that BASEPLANE can be parametrized to satisfy the following properties:

1. For every cut node  $u$ , we reserve a dimension in  $\mathbf{h}_u^L$  that stores the number of cut nodes in  $\delta_u$ . This is done in the UPDATE part of the corresponding layer.
2. There is a bijection  $\lambda$  between the representations of the induced subtrees and subtree codes, such that  $\lambda(\mathbf{h}_{\delta_u}^{(L)}) = \text{CODE}(\delta_u)$  and  $\lambda^{-1}(\text{CODE}(\delta_u^{(L)})) = \mathbf{h}_{\delta_u}^{(L)}$ , for cut nodes  $u$  that have strictly less than  $L$  cut nodes in  $\delta_u$ .
3. There is a bijection  $\rho$  between the cut node representations and subtree codes, such that  $\rho(\mathbf{h}_u^{(L)}) = \text{CODE}(\delta_u)$  and  $\rho^{-1}(\text{CODE}(\delta_u^{(L)})) = \mathbf{h}_u^{(L)}$ , for cut nodes  $u$  that have strictly less than  $L$  cut nodes in  $\delta_u$ .

Observe that the property (2) directly gives us a complete graph invariant for each subtree  $\delta_u$  induced by each cut node  $u$ , since the codes for every induced subtree are complete, and through the bijection, we obtain complete representations. The remaining properties are useful for later in order to obtain a more efficient construction.

The UPDATE function in every layer is crucial for our constructions, and we recall its definition:

$$\mathbf{h}_u^{(\ell)} = f^{(\ell)}\left(g_1^{(\ell)}\left(\mathbf{h}_u^{(\ell-1)} + \sum_{v \in N_u} \mathbf{h}_v^{(\ell-1)}\right) \parallel g_2^{(\ell)} \sum_{v \in V} \mathbf{h}_v^{(\ell-1)} \parallel g_3^{(\ell)}\left(\mathbf{h}_u^{(\ell-1)} + \sum_{B \in \pi_u^G} \mathbf{h}_B^{(\ell)}\right) \parallel g_4^{(\ell)}\left(\mathbf{h}_u^{(\ell-1)} + \sum_{C \in \sigma_u^G} \mathbf{h}_C^{(\ell)}\right) \parallel \mathbf{h}_{\delta_u}^{(\ell)}\right).$$

We prove that there exists a parametrization of BASEPLANE which satisfies the properties (1)–(3) by induction on the number of layers  $L$ .

**Base case.**  $L = 1$ . In this case, there are no cut nodes satisfying the constraints, and the model trivially satisfies the properties (2)–(3). To satisfy (1), we can set the inner MLP in CUTENC as the identity function, and the outer MLP as a function which adds 1 to the first dimension of the input embedding. This ensures that the representations  $\mathbf{h}_{\delta_u}^{(1)}$  of cut nodes  $u$  have their first components equal to the number of cut nodes in  $\delta_u$ . We can encode the property (1) in  $\mathbf{h}_u^{(\ell)}$  using the representation  $\mathbf{h}_{\delta_u}^{(1)}$ , since the latter is a readout component in UPDATE.

**Inductive step.**  $L > 1$ . By induction hypothesis, there is an  $(L - 1)$ -layer parametrization of BASEPLANE which satisfies the properties (1)–(3). We can define the  $L$ -th layer so that our  $L$  layer parametrization of BASEPLANE satisfies all the properties:

*Property (1):* For every cut node  $u$ , the function UPDATE has a readout from  $\mathbf{h}_u^{(L-1)}$  and  $\mathbf{h}_{\delta_u}^{(L)}$ , which allows us to copy the first dimension of  $\mathbf{h}_u^{(L-1)}$  into the first dimension of  $\mathbf{h}_u^{(L)}$  using a linear transformation, which immediately gives us the property.

*Property (2):* For this property, let us first consider the easier direction. Given the code of  $\delta_u$ , we want to find the CUTENC representation for the induced subtree of  $u$ . From the subtree code, we can reconstruct the induced subtree  $\delta_u$ , and then run a  $L$ -layer BASEPLANE on reconstructed Block-Cut Tree to find the CUTENC representation. As for the other direction, we want to find the subtree code of given the representation of the induced subgraph. The CUTENC encodes a multiset  $\{\{\mathbf{h}_B, \{\mathbf{h}_v | v \in \chi(B)\}\} | B \in \chi(u)\}$ . By induction hypothesis, we know that all grandchildren  $v \in \chi^2(u)$  already have properties (1)–(3) satisfied for them with the first  $(L - 1)$  layers. Hence, using the parametrization of TRIENC and BIENC given in Lemma 6.2, as part of the  $L$ -th BASEPLANE layer, we can get a bijection between BICODE and biconnected component representation. This way we can obtain BICODE( $B$ ) for all the children biconnected components  $B \in \chi(u)$ , with all the necessary overriding. Having all necessarily overrides is crucial, because to get the KHC code for the cut node  $u$ , we need to concatenate the biconnected codes from 10 that already have the required overrides. Hence, we make the parametrization of CUTENC encode multisets of representations for biconnected components  $B \in \chi(u)$ , and by similar arguments as in the proof of Lemma 6.2, this can be done using the MLPs in CUTENC.

*Property (3):* Using the bijection from (2) as a bridge, we can easily show the property (3). In the update formula, we appended  $\mathbf{h}_{\delta_u}^{(L)}$  using the MLP. If the MLP is bijective with the dimension taken by  $\mathbf{h}_{\delta_u}^{(L)}$ , we get a bijection between the node representation and the subtree representation. By transitivity, we get a bijection between node representations and subtree codes.

This concludes our construction using  $L = O(n)$  BASEPLANE layers.

**Efficient construction.** We now show that the presented construction can be made more efficient, using only  $L = \lceil \log_2(n) \rceil + 1$  layers. This is achieved by treating the cut nodes  $u$  differently based on the number of cut nodes they include in their induced subtrees  $\delta_u$ . In this construction, the property (1) remains the same, but the properties (2)–(3) are modified:

1. For every cut node  $u$ , we reserve a dimension in  $\mathbf{h}_u^{(L)}$  that stored to the number of cut nodes in  $\delta_u$ . This is done in the UPDATE part of the corresponding layer.
2. There is a bijection  $\lambda$  between the representations of the induced subtrees and subtree codes, such that  $\lambda(\mathbf{h}_{\delta_u}^{(L)}) = \text{CODE}(\delta_u)$  and  $\lambda^{-1}(\text{CODE}(\delta_u^{(L)})) = \mathbf{h}_{\delta_u}^{(L)}$ , for cut nodes  $u$  that have strictly less than  $2^{(L-1)}$  cut nodes in  $\delta_u$ .

3. There is a bijection  $\rho$  between the cut node representations and subtree codes, such that  $\rho(\mathbf{h}_u^{(L)}) = \text{CODE}(\delta_u)$  and  $\rho^{-1}(\text{CODE}(\delta_u^{(L)})) = \mathbf{h}_u^{(L)}$ , for cut nodes  $u$  that have strictly less than  $2^{(L-1)}$  cut nodes in  $\delta_u$ .

In this construction, we treat the cut nodes  $u$  which have strictly less than  $2^{L-1}$  cut nodes in their induced subtrees  $\delta_u$ , differently than the other cut nodes. In the first case, we consider an arbitrary cut node  $u$  with less than  $2^{L-1}$  cut nodes in  $\delta_u$ . In this case, the same arguments apply as before. As for the second case, we observe the following: there is at most one grandchild  $v_1 \in \chi^2(u)$  with at least  $2^{L-2}$  cut nodes in  $\delta_{v_1}$ , as otherwise  $u$  would have at least  $2^{L-1}$  cut nodes in it. Using the same argument for  $v_1$ , there is at most one  $v_2 \in \chi^2(v_1)$  with at least  $2^{L-2}$  cut nodes in  $\delta_{v_2}$ . By repeating this until there are no grandchildren with at least  $2^{L-2}$  cut nodes in their subtree, we can form a sequence of cut nodes  $u = v_0, v_1, \dots, v_k$ , such that  $v_{i+1}$  is a grandchild of  $v_i$  for all  $0 \leq i < k$ . By induction hypothesis, all other cut nodes in  $\delta_u$  already satisfy properties (2) and (3). Furthermore, we already know that the earlier parametrization ensures that the properties will hold for  $v_k$ . We will now extend this parametrization to ensure that the properties will also hold for the other nodes in this sequence, by modifying CUTENC. Because of the bottom up nature of CUTENC, when encoding  $v_i$  for  $0 \leq i < k$ , we will already have the new representation  $\mathbf{h}_{\delta_{v_{i+1}}}^{(L)}$ . Furthermore, since there is

exactly one grandchild that does not satisfy the required properties, only one representation  $\mathbf{h}_B^{(L)}$  of a child biconnected component  $B \in \chi(v_i)$  will not satisfy properties (2) and (3) after  $L - 1$  layers. However, in CUTENC, we also have access to the representations of induced subtrees from cut nodes (in the summation before the inner MLP), so it suffices to encode this sequence of cut nodes separately, so that we will be able to distinguish  $\mathbf{h}_{\gamma_{v_{i+1}}}^{(L)}$  from the rest of the subtrees induced by grandchildren (because the new representation  $\mathbf{h}_{\gamma_{v_{i+1}}}^{(L)}$  already satisfies the properties). This can be done in a single BASEPLANE layer where the only difference between this construction and the less efficient one is that we need reserve one layer which is parametrized differently than the other layers to handle the cut nodes in this sequence.  $\square$

**Theorem 6.1.** *For any planar graphs  $G_1 = (V_1, E_1, \zeta_1)$  and  $G_2 = (V_2, E_2, \zeta_2)$ , there exists a parametrization of BASEPLANE with at most  $L = \lceil \log_2(\max\{|V_1|, |V_2|\}) \rceil + 1$  layers, which computes a complete graph invariant, that is, the final graph-level embeddings satisfy  $\mathbf{z}_{G_1}^{(L)} \neq \mathbf{z}_{G_2}^{(L)}$  if and only if  $G_1$  and  $G_2$  are not isomorphic.*

*Proof.* The “only if” direction is immediate because BASEPLANE is an invariant model for planar graphs. To prove the “if” direction, we do a case analysis on the root of the two Block-Cut Trees. For each case, we provide a parametrization of BASEPLANE such that  $\mathbf{z}_{G_1}^{(L)} \neq \mathbf{z}_{G_2}^{(L)}$  for any two non-isomorphic graphs  $G_1$  and  $G_2$ . A complete BASEPLANE model can be obtained by appropriately unifying the respective parametrizations.

**Case 1.**  $\text{ROOT}(\delta_1)$  and  $\text{ROOT}(\delta_2)$  represents two cut nodes.

Consider a parametrization of the final BASEPLANE update formula, where only cut node representation is used, and a simplified readout function that only aggregates from the last layer. We can rewrite the readout for a graph in terms of the cut node representation from the last BASEPLANE layer.

$$\mathbf{z}_G^{(L)} = \text{MLP} \left( \sum_{u \in V^G} \text{MLP}(\mathbf{h}_{\delta_u}^{(L)}) \right).$$

Let  $\text{CUT}(G) = \{\{\mathbf{h}_{\delta_u}^{(L)} \mid u \in V^G\}\}$ . Intuitively,  $\text{CUT}(G)$  is a multiset of cut node representations from the last BASEPLANE layer. We assume  $|V_{\delta_1}| \leq |V_{\delta_2}|$  without loss of generality. Consider the root node  $\text{ROOT}(\delta_2)$  of the Block-Cut Tree  $\delta_2$ . By Lemma 6.3, we have  $\mathbf{h}_{\text{ROOT}(\delta_2)}$  as a complete graph invariant with  $L$  layers. Since  $\delta_2$  cannot appear as a subtree of  $\delta_1$ ,  $\mathbf{h}_{\text{ROOT}(\delta_2)} \notin \text{CUT}(G_1)$ . Hence,  $\text{CUT}(G_1) \neq \text{CUT}(G_2)$ . Since this model can define an injective mapping on the multiset  $\text{CUT}(G)$  using similar arguments as before, we get that  $\mathbf{z}_{G_1}^{(L)} \neq \mathbf{z}_{G_2}^{(L)}$ .

**Case 2.**  $\text{ROOT}(\delta_1)$  and  $\text{ROOT}(\delta_2)$  represents two biconnected components.

We use a similar strategy to prove Case 2. First, we consider a simplified BASEPLANE model, where the update formula considers biconnected components only and the final readout aggregates from the last BASEPLANE layer. We similarly give the final graph readout in terms of the biconnected component representation from the last BASEPLANE layer.

$$z_G = \text{MLP} \left( \sum_{u \in V^G} \text{MLP} \left( \mathbf{h}_u^{(L-1)} + \sum_{B \in \pi_u^G} \mathbf{h}_B^{(L)} \right) \right).$$

Let  $\text{BC}(G) = \{(\mathbf{h}_u^{(L-1)}, \{\{\mathbf{h}_B^{(L)} \mid B \in \pi_u^G\}\}) \mid u \in V^G\}$ . In Lemma 6.3, we prove that  $\mathbf{h}_B^{(L)}$  is also a complete invariant for the subtree rooted at  $B$  in the Block-Cut Tree. First, we show  $\text{BC}(G_1) \neq \text{BC}(G_2)$ . As before, we assume  $|V_{\delta_1}| \leq |V_{\delta_2}|$  without loss of generality. Consider how the biconnected component representation  $\mathbf{h}_{\text{ROOT}(\delta_2)}$  appears in the two multisets of pairs. For  $G_2$ , there exist at least one node  $u$  and pair:

$$(\mathbf{h}_u^{(L-1)}, \{\{\mathbf{h}_B^{(L)} \mid B \in \pi_u^G\}\}) \in \text{BC}(G_2),$$

such that  $\mathbf{h}_{\text{ROOT}(\delta_2)} \in \{\{\mathbf{h}_B^{(L)} \mid B \in \pi_u^G\}\}$ . However, because  $\mathbf{h}_{\text{ROOT}(\delta_2)}$  is a complete invariant for  $\delta_2$  and  $\delta_2$  cannot appear as a subtree in  $\delta_1$ , no such pair exists in  $\text{BC}(G_1)$ . Given  $\text{BC}(G_1) \neq \text{BC}(G_2)$ , we can parameterize the MLPs to define an injective mapping to get that  $z_{G_1}^{(L)} \neq z_{G_2}^{(L)}$ .

**Case 3.**  $\text{ROOT}(\delta_1)$  represents a cut node and  $\text{ROOT}(\delta_2)$  represents a biconnected component.

We can distinguish  $G_1$  and  $G_2$  using a simple property of  $\text{ROOT}(\delta_1)$ . Recall that  $\pi_u^G$  represents the set of biconnected components that contains  $u$ , and  $\chi^\delta(C)$  represents the  $C$ 's children in the Block-Cut Tree  $\delta$ . For  $\text{ROOT}(\delta_1)$ , we have  $|\pi_u^{G_1}| = |\chi^{\delta_1}(u)|$ . However, for any other cut node  $u$ , including the non-root cut node in  $\delta_1$  and all cut nodes in  $\delta_2$ , we have  $|\pi_u^G| = |\chi^\delta(u)| + 1$ , because there must be a parent node  $v$  of  $u$  such that  $v \in \pi_u^{G_1}$  but  $v \notin \chi^\delta(u)$ .

Therefore, we consider a parametrization of a one-layer BASEPLANE model that exploits this property. In BiENC, we have a constant vector  $[1, 0]^\top$  for all biconnected components. In CUTENC, we learn  $[0, |\chi_u|]^\top$  for all cut nodes  $u$ . In the update formula, we have  $[|\pi_u^G| - |\chi^\delta(u)| - 1, 0]^\top$ . All of the above specifications can be achieved using linear maps. For the final readout, we simply sum all node representations with no extra transformation.

Then, for  $\text{ROOT}(\delta_1)$ , we have  $\mathbf{h}_{\text{ROOT}\delta_u} = [-1, 0]^\top$ . For any other cut node  $u$ , we have  $\mathbf{h}_u = [0, 0]^\top$ . For all non-cut nodes  $u$ , we also have  $\mathbf{h}_u = [0, 0]^\top$  because  $|\pi_u^G| = 1$  and  $\mathbf{h}_{\delta_u} = [0, 0]^\top$ . Summing all the node representations yields  $z_{G_1} = [-1, 0]^\top$  but  $z_{G_2} = [0, 0]^\top$ . Hence, we obtain  $z_{G_1}^{(L)} \neq z_{G_2}^{(L)}$ , as required.  $\square$

## C Further experimental details

### C.1 Link to code

The code for our experiments, as well as instructions to reproduce our results and set up dependencies, can be found at this anonymized GitHub repository: <https://github.com/ZZYSonny/Plane>

### C.2 Computational resources

We run all experiments on 4 cores from Intel Xeon Platinum 8268 CPU @ 2.90GHz with 32GB RAM. In Table 5, we report the approximate time to train a BASEPLANE model on each dataset and with each tuned hidden dimension value.

### C.3 Distinguishing graphs on EXP

**Experimental setup.** In this experiment, we evaluate the BASEPLANE model on the planar EXP benchmark [1] and compare with standard MPNNs, as well as MPNNs with random node initialization

Table 5: Approximate Training Time for BASEPLANE

Dataset Name	Hidden Dimension	Training Time (hours)
QM9 <sub>CC</sub>	32	2.5
MolHIV	64	6
QM9	128	25
ZINC(12k)	64	5
	128	8
ZINC(Full)	128	45
EXP	32	0.2

and higher-order GNNs. The EXP dataset consists of a set of planar graphs which each represent a satisfiability problem (SAT) instance. These instances are grouped into pairs, such that these pairs cannot be distinguished by 1-WL, and lead to different SAT outcomes. The task in this dataset is to predict the satisfiability of each instance. Therefore, to obtain above-random performance on this dataset, a model must have a sufficiently strong expressive power (2-WL or more).

To conduct this experiment, we use a 2-layer BASEPLANE model with 64-dimensional node embeddings. We instantiate the tri-connected component encoder with 16-dimensional positional encodings, each computed using a periodicity of 64. We follow the same protocol as the original work: we use 10-fold cross validation on the dataset, train BASEPLANE on each fold for 50 epochs using the Adam [39] optimizer with a learning rate of  $10^{-3}$ , and binary cross entropy loss.

**Results.** The results of PlanE and other baselines on the EXP dataset are reported in Table 6. As expected, PlanE almost perfectly solves the task, achieving a performance exceeding 99% despite not using any external components, e.g., random features, or computationally intractable methods, e.g. higher-order GNNs. In fact, the model solely relies on classical algorithm component decompositions, and does not rely on explicitly selected and designed features, to achieve this performance gain. Therefore, this experiment highlights that the general algorithmic decomposition effectively improves expressiveness in a practical machine learning setup, and leads to strong PlanE performance on EXP, where a standard MPNN would otherwise fail.

Table 6: Accuracy results on the EXP synthetic benchmark. Baselines are as reported in the original paper [1].

Model	Accuracy (%)
GCN-RNI(N)	<b>98.0</b> $\pm 1.85$
1-2-3-GCN-L	50.0
<b>3-GCN</b>	<b>99.7</b> $\pm 0.004$
BASEPLANE	<b>100.0</b> $\pm 0.0$

#### C.4 E-BASEPLANE architecture

E-BASEPLANE builds on BASEPLANE, and additionally processes edge features within the input graph. To this end, it supersedes the original BASEPLANE update equations for SPQR components and nodes with the following analogs:

$$\begin{aligned}
 \mathbf{h}_C^{(\ell)} &= \text{MLP} \left( \sum_{i=1}^{|\omega|} \text{MLP}(\mathbf{h}_{\omega[i]}^{(\ell-1)} \parallel \hat{\mathbf{h}}_{\omega[i], \omega[(i+1)\%|\omega]}^{(\ell-1)} \parallel \mathbf{p}_{\kappa[i]} \parallel \mathbf{p}_i) \right), \text{ and} \\
 \mathbf{h}_u^{(\ell)} &= f^{(\ell)} \left( g_1^{(\ell)}(\mathbf{h}_u^{(\ell-1)} + \sum_{v \in N_u} g_5^{(\ell)}(\mathbf{h}_v^{(\ell-1)} \parallel \mathbf{h}_{v,u}^{(\ell-1)})) \parallel g_2^{(\ell)} \sum_{v \in V} \mathbf{h}_v^{(\ell-1)} \right. \\
 &\quad \left. g_3^{(\ell)}(\mathbf{h}_u^{(\ell-1)} + \sum_{B \in \pi_u^G} \mathbf{h}_B^{(\ell)}) \parallel g_4^{(\ell)}(\mathbf{h}_u^{(\ell-1)} + \sum_{T \in \tau_u^G} \mathbf{h}_T^{(\ell)}) \parallel \mathbf{h}_{\delta_u}^{(\ell)} \right),
 \end{aligned}$$

where  $\hat{\mathbf{h}}_{i,j} = \mathbf{h}_{i,j}$  if  $(i, j) \in E$  and is the ones vector ( $\mathbf{1}^d$ ) otherwise



## C.5 Training setups

**Clustering coefficient of QM9 graphs.** To train all baselines, we use the Adam optimizer with a learning rate from  $\{10^{-3}; 10^{-4}\}$ , and train all models for 100 epochs using a batch size of 256 and L2 loss.

**Graph classification on MolHIV.** We instantiate E-BASEPLANE with an embedding dimension of 64 and a positional encoding dimensionality of 16. We further tune the number of layers within the set  $\{2, 3\}$  and use a dropout probability from the set  $\{0, 0.25, 0.5, 0.66\}$ . Furthermore, we train our models with the Adam optimizer [39], with a constant learning rate of  $10^{-3}$ . Finally, we perform training with a batch size of 256 and train for 300 epochs.

**Graph regression on QM9.** As standard, we train E-BASEPLANE using mean squared error (MSE) and report mean absolute error (MAE) on the test set. For training E-BASEPLANE, we tune the learning rate from the set  $\{10^{-3}, 5 \times 10^{-4}\}$  with the Adam optimizer, and adopt a learning rate decay of 0.7 every 25 epochs. Furthermore, we use a batch size of 256, 128-dimensional node embeddings, and 32-dimensional positional encoding.

**Graph regression on ZINC.** In all experiments, we use a node embedding dimensionality from the set  $\{64, 128\}$ , use 3 message passing layers, and 16-dimensional positional encoding vectors. We train both BASEPLANE and E-BASEPLANE with the Adam optimizer [39] using a learning rate from the set  $\{10^{-3}, 5 \times 10^{-4}, 10^{-4}\}$ , and follow a decay strategy where the learning rate decays by a factor of 2 for every 25 epochs where validation loss does not improve. We train using a batch size of 256 in all experiments, and run training using L1 loss for 500 epochs on the ZINC subset, and for 200 epochs on the full ZINC dataset.